

**Universidade Federal do Rio Grande – FURG**  
**Instituto de Oceanografia**  
Programa de Pós-Graduação em Oceanologia

**VARIABILIDADE ESPAÇO-TEMPORAL DAS  
CONCENTRAÇÕES DE SEDIMENTO EM  
SUSPENSÃO NA LAGOA DOS PATOS**

LILIANE PARANHOS BITENCOURT

Dissertação apresentada a  
coordenação do PPGOCFQG  
como requisito parcial para a  
obtenção do título de mestre

Orientadora: *Prof<sup>ª</sup>. Dr<sup>ª</sup>.* ELISA HELENA FERNANDES

Universidade Federal do Rio Grande (FURG), Brasil

Rio Grande, RS, Brasil

Abril, 2019.

# **VARIABILIDADE ESPAÇO-TEMPORAL DAS CONCENTRAÇÕES DE SEDIMENTO EM SUSPENSÃO NA LAGOA DOS PATOS**

Dissertação apresentada ao Programa de Pós-Graduação em Oceanologia,  
como parte dos requisitos para a obtenção do Título de Mestre.

por

**LILIANE PARANHOS BITENCOURT**

Rio Grande, RS, Brasil

Abril, 2019.

© A cópia parcial e a citação de trechos desta tese são permitidas sobre a condição de que qualquer pessoa que a consulte reconheça os direitos autorais do autor. Nenhuma informação derivada direta ou indiretamente desta obra deve ser publicada sem o consentimento prévio e por escrito do autor.

BITENCOURT, LILIANE PARANHOS

Variabilidade espaço-temporal das concentrações de sedimento em suspensão na Lagoa dos Patos / Liliane Paranhos Bitencourt. – Rio Grande: FURG, 2019.

Número de páginas 66p.

Dissertação (Mestrado) – Universidade Federal do Rio Grande. Mestrado/Doutorado em Oceanologia. Área de Concentração: Oceanografia Física.

1. Concentração de Sedimento em Suspensão. 2. Lagoa dos Patos. 3. Modelagem Numérica. I. Variabilidade espaço-temporal das concentrações de sedimento em suspensão na Lagoa dos Patos.

## **Agradecimentos**

Primeiramente, gostaria de agradecer à minha família por todo amor, paciência, confiança e suporte e, principalmente, por não desistirem de mim nos momentos mais difíceis. Em especial, gostaria de agradecer à minha mãe Luciane, por todo amor e perseverança, sempre me puxando para frente e nunca me deixando desistir dos meus objetivos; ao meu pai Paulo, que de sua forma singular, foi importante para mim e para a minha formação.

À minha irmã Letícia, que mesmo com todas as brigas, me ajudou, deu amor e nunca desistiu de mim; e a minha sobrinha Isabelle, minha princesa e amor da minha vida, por todo amor e por, desde tão pequena, já acreditar no meu potencial e me ver como exemplo. Além da Floribella e do Bobó, meus cachorros, por serem tão amorosos e ficarem ao meu lado nas noites em claro de estudos. Todos vocês e os não citados tem uma parcela significativa nessa conquista.

À minha orientadora, Elisa Fernandes, por ter dado essa e outras oportunidades de trabalho, onde tanto cresci e tirei diversas lições, não só para o trabalho, mas também para a vida; por ter acreditado no meu potencial e me feito sempre querer ser melhor. E também aos meus companheiros do LOCOSTE por terem me aturado por todos esses anos, me auxiliado nas minhas dúvidas e, até mesmo, nesse trabalho, além de, é claro, do ótimo ambiente de trabalho que temos no laboratório.

A todos os meus amigos por todo amor, companheirismo e suporte ao longo da minha jornada acadêmica, em especial para a minha melhor amiga Myllena que, mesmo com a distância, esteve sempre presente e me auxiliando no que fosse preciso.

À Coordenação de Aperfeiçoamento de Pessoal de Ensino Superior (CAPES) pela bolsa de estudos concedida.

# Índice

<b>Agradecimentos</b> .....	4
<b>Lista de Figuras da Dissertação</b> .....	6
<b>Lista de Figuras do Manuscrito</b> .....	7
<b>Resumo</b> .....	10
<b>Abstract</b> .....	11
<b>Capítulo I: Introdução</b> .....	12
<b>Capítulo II: Objetivos</b> .....	20
<b>Capítulo III: Materiais e Métodos</b> .....	22
<b>Capítulo IV: Resultados e Discussões</b> .....	33
<b>1. Introduction</b> .....	34
<b>2. Data and Methods</b> .....	36
2.1. Study area .....	36
2.2. Field Data .....	38
2.3. Numerical Model.....	39
2.4. Calibration and Validation .....	41
2.5. Climate and precipitation data.....	43
2.6. Wavelets .....	43
<b>3. Results and Discussion</b> .....	44
3.1. <i>SSC Variability</i> .....	44
3.2. <i>The estuarine behaviour</i> .....	50
3.3. <i>SSC Spatio-Temporal Variability</i> .....	53
3.4. <i>Future Studies</i> .....	56
<b>4. Conclusions</b> .....	57
<b>Capítulo V: Considerações Finais</b> .....	59
<b>Referências Bibliográficas</b> .....	62

## Lista de Figuras da Dissertação

<b>Figura 1.</b> Área de estudo. Os pontos azuis representam os principais afluentes da Lagoa dos Patos: Rio Guaíba (ao norte), Rio Camaquã (porção central) e Canal São Gonçalo (ao sul).....	16
<b>Figura 2.</b> Representação esquemática das ações dos ventos de (A) nordeste e (B) sudoeste na Lagoa dos Patos (Castelão e Möller, 2003).....	17
<b>Figura 3.</b> Sedimentos de fundo do: A) corpo lagunar (Toldo Jr <i>et al</i> , 2006) e B) corpo estuarino (Callari, 1980).....	18
<b>Figura 4.</b> Malha Batimétrica.....	28
<b>Figura 5.</b> Campo inicial de salinidade para todo o domínio.....	29
<b>Figura 6.</b> Série temporal de intensidade do vento para o período estudado....	30
<b>Figura 7.</b> Série temporal da vazão do Rio Guaíba, Rio Camaquã e Canal São Gonçalo para o período estudado (2002-2006).....	31

## Lista de Figuras do Manuscrito

- Figure 1.** Study area. Blue dots show the geographic position of Patos Lagoon major tributaries, and red dots represent points from where model results were extracted in the study area (Figure 7).....38
- Figure 2.** Numerical Mesh of the model domain and identification of initial and boundary conditions for the TELEMAC-3D model.....40
- Figure 3.** Comparison between in situ (red) and model (black) data of: (a) surface and (b) bottom velocities; (c) SSC; (d) surface and (e) bottom salinities for January 2006.....43
- Figure 4.** Temporal evolution of calculated SSC and river discharge for the 5-years period at a) Guaíba River, b) Camaquã River, and c) São Gonçalo Channel. Wind speed is shown in d, where negative (positive) values represent NE (SW) winds. Monthly mean timeseries (2002-2006) of SSC (black,  $\text{mg.L}^{-1}$ ) at e) Guaíba River, f) Camaquã River, and g) São Gonçalo Channel. Standard deviations are shown in grey shading for SSC.....46
- Figure 5.** Five years (2002-2006) calculated SSC means for the austral seasons: a) summer (DJF), b) fall (MAM), c) winter (JJA), and d) spring (SON). Zoom for the estuarine are shown for e) summer, f) fall, g) winter, and h) spring.....47
- Figure 6.** Influence of winds on SSC behaviour.....48
- Figure 7.** a) Spatio-temporal distribution of SSC ( $\text{mg.L}^{-1}$ ) along the Patos Lagoon (see Figure 1 for location). b) Guaíba River discharge anomaly. Positive (negative) Guaíba river outflow anomaly is shown in blue (red). c) wind speed, where negative (positive) values represent NE (SW) winds; d) precipitation rates (black), its mean (blue) and long-term trend (red); and e) SOI index and its long-term trend (black). Dashed lines between -0.7 and 0.7 represent periods of neutral years.....49
- Figure 8.** a) Water level differences between points 8 and 2 (see Figure 1 for location). Ebb (Flood) events are presented in blue (red). b) Wind speed. Negative (Positive) values shown in blue (red) represent NE (SW) winds; c) calculated SSC data for points 2 and 8.....51
- Figure 9.** Spatial and temporal variations of calculated SSC and salinities at points (a) 8, (b) 6, (c) 4, and (d) 2 for the simulated period (2002-2006).....53

**Figure 10.** At P2: a) Time series of the river discharge (black) and SSC (red). (b) Local energy cross-spectrum using the Mexican hat wavelet. The contour lines enclose regions with 95% confidence interval. The dashed line indicates the cone of influence where the edge effects become important. (c) The time-averaged wavelet power spectra. The dashed line represents the 95% confidence level. (d) Time series of wind intensity (black) and SSC (red). (e) Local energy cross-spectrum using the Morlet wavelet. The contour lines enclose regions with 95% confidence interval. The dashed line indicates the cone of influence where the edge effects become important. (f) The time-averaged wavelet power spectra. The dashed line represents the 95% confidence level.....54

**Figure 11.** At P8: A) Time series of the river discharge (black) and SSC (red). (b) Local energy cross-spectrum using the Mexican hat wavelet. The contour lines enclose regions with 95% confidence interval. The dashed line indicates the cone of influence where the edge effects become important. (c) The time-averaged wavelet power spectra. The dashed line represents the 95% confidence level. (d) Time series of wind intensity (black) and SSC (red). (e) Local energy cross-spectrum using the Morlet wavelet. The contour lines enclose regions with 95% confidence interval. The dashed line indicates the cone of influence where the edge effects become important. (f) The time-averaged wavelet power spectra. The dashed line represents the 95% confidence level. ....55

**Figure 12.** At P24: A) Time series of the river discharge (black) and SSC (red). (b) Local energy cross-spectrum using the Mexican hat wavelet. The contour lines enclose regions with 95% confidence interval. The dashed line indicates the cone of influence where the edge effects become important. (c) The time-averaged wavelet power spectra. The dashed line represents the 95% confidence level. (d) Time series of wind intensity (black) and SSC (red). (e) Local energy cross-spectrum using the Morlet wavelet. The contour lines enclose regions with 95% confidence interval. The dashed line indicates the cone of influence where the edge effects become important. (f) The time-averaged wavelet power spectra. The dashed line represents the 95% confidence level.....56



## **Lista de Tabelas**

<b>Table 1.</b> Classification of errors (Walstra <i>et al.</i> , 2001).....	41
<b>Table 2.</b> Best set of physical parameters used in the calibration exercise.....	42
<b>Table 3.</b> Statistical analysis between SSC and Salinity.....	52

## Resumo

A Lagoa dos Patos, localizada no extremo sul do Brasil, é uma lagoa rasa e turva de grande importância ecológica e econômica. A variabilidade sazonal, anual e interanual das concentrações de sedimento em suspensão (CSS) dessa lagoa foi investigada através de cinco anos (2002-2006) de simulações hidrodinâmicas + transporte de sedimento em suspensão a partir do modelo hidrodinâmico TELEMAC – 3D. O modelo foi calibrado e validado através da comparação entre seus resultados e dados in situ de velocidade de corrente, salinidade e CSS, e indicou uma performance excelente. Em seguida, os resultados do modelo foram combinados com dados de descarga dos rios, vento, taxas de precipitação e índices climáticos (ENSO) para identificar as suas influências nas CSS ao longo da lagoa. A relação entre séries temporais diárias de CSS e descarga dos rios foi alta ( $r \approx 0.80$ ), indicando uma forte correlação entre essas séries temporais na Lagoa dos Patos. A variabilidade sazonal de CSS indicou altas SSC durante o inverno e a primavera, e CSS moderadas a baixas durante o verão e o outono, demonstrando uma relação com o padrão de descarga dos rios. Em escala interanual, a influência dos eventos ENSO gerou altos valores de CSS ao longo da lagoa, principalmente durante os anos de El Niño e próximo às desembocaduras dos tributários, enquanto o padrão oposto foi observado durante os anos de La Niña. Diante disso, a Lagoa dos Patos se mostra como um sistema dinâmico, e as CSS são principalmente controladas pelas descargas dos rios em escalas maiores de tempo e moduladas pela ação do vento em escalas mais curtas.

*Palavras-chave:* Concentração de Sedimento em Suspensão, Lagoa dos Patos, ENSO, Modelagem Numérica, TELEMAC-3D.

## **Abstract**

The Patos Lagoon, located in the Southernmost part of Brazil, is a shallow and turbid lagoon of huge ecological and economical importance. The seasonal, annual, and interannual variability of suspended sediment concentrations (SSC) of this lagoon was investigated based on five years (2002-2006) of hydrodynamics + SSC simulations with the TELEMAC – 3D hydrodynamic model. The model was initially calibrated and validated by comparing results with in situ current velocities, salinity, and SSC measurements, indicating an excellent performance. Afterwards, modelling results were combined with river discharge, wind, precipitation rates, and climate index (ENSO) data to identify their influence on SSC throughout the lagoon. The relation between daily timeseries of SSC and river discharge was high ( $r \approx 0.80$ ), indicating a strong correlation between these time series in the Patos Lagoon. SSC seasonal variability was also observed, with high SSC from winter to spring, and moderate to low SSC during summer and fall, indicating a relation with the river discharge pattern. On the interannual variability scale, the ENSO influence promoted high SSC values throughout the lagoon, mainly during El Niño years and near the tributaries mouth, while the opposite pattern was observed during La Niña years. Thus, the Patos Lagoon is a dynamic system and SSC are mainly controlled by river discharges at longer timescales and modulated by the wind action at shorter timescales.

*Keywords:* Suspended Sediment Concentration, Patos Lagoon, ENSO, numerical modelling, TELEMAC-3D.

# Capítulo I:

## Introdução

## 1. Introdução

Por serem a interface oceano-continente, as regiões costeiras apresentam grande importância econômica e ambiental, uma vez que diversas atividades socioeconômicas e de lazer são desenvolvidas nesses ambientes (Petti *et al.*, 2018) e, também, por servirem de local para reprodução e/ou desenvolvimento de organismos. Além disso, devido a sua localização, estão constantemente suscetíveis a fenômenos resultantes da variabilidade climática, tais como aumento do nível do mar e eventos ENSO.

Essas regiões são permanentemente remodeladas pela ação dos rios, ventos, marés e topografia (Fossati e Piedra-Cueva, 2008; Garvine, 1975; Gong e Shen, 2011). Dentre as variáveis afetadas por esta dinâmica, encontram-se os sedimentos de fundo e em suspensão, que estão sujeitos a diferentes processos de transporte sedimentar, sendo erodidos, advectados, depositados e consolidados. As partículas menores (silte e argila) tendem a permanecer em suspensão e atingem maiores distâncias até serem depositadas.

A presença desses sedimentos em suspensão no ambiente serve como indicador da qualidade ambiental (Etemad-Shahidi *et al.*, 2010), uma vez que afetam a penetração de luz na coluna d'água e, por conseguinte, os organismos que dela dependem. Ainda, os sedimentos coesivos, devido a sua capacidade de agregação, desempenham papel importante no transporte de contaminantes, além de também servirem como fonte de sedimento para região costeira adjacente (Milliman and Meade, 1983). Portanto, se faz necessário conhecer o padrão de distribuição dos sedimentos por diversos motivos, tais como as taxas de exportação de sedimentos provenientes dos rios para os oceanos e, também, a otimização das operações de dragagens, assim como a extensão da contaminação de certos compostos e o ciclo de vida de diversos peixes.

Apesar de importante, compreender a variabilidade espaço-temporal dos sedimentos em suspensão em ambientes costeiros se torna uma tarefa muitas vezes complexa, principalmente em ambientes onde essas distribuições são altamente variáveis tanto no tempo quanto no espaço. Métodos tradicionais de

coletas de dados, entretanto, se tornam difíceis, uma vez que apresentam altos custos operacionais, requerem logísticas muitas vezes complexas e, também, por serem espaço-temporalmente limitados (Vantrepotte *et al.*, 2011). Dessa forma, verifica-se a necessidade de buscar ferramentas que consigam superar essas limitações e que, ao mesmo tempo, consigam fornecer informações confiáveis a respeito dos processos envolvidos.

Por conta disso, a modelagem numérica se torna uma excelente alternativa, uma vez que os custos são menores e a cobertura espacial e temporal pode ser muito maior (Krajewski *et al.*, 2017), além de conseguir reproduzir a alta complexidade dos fenômenos que se deseja estudar. Diversos estudos utilizando a modelagem numérica para compreender a variabilidade das concentrações de sedimentos em suspensão têm sido realizados no mundo (Villaret e Trowbridge, 1991; Lumborg *et al.*, 2003; Wang *et al.*, 2007; Marques *et al.*, 2010; Silva *et al.*, 2015; Krajewski *et al.*, 2017; Santoro *et al.*, 2017). Entretanto, eles apenas abordam pequenas escalas de tempo, o que não permite determinar os padrões de sedimento sujeitos a variabilidade climática, por exemplo.

A modelagem de sedimentos coesivos envolve diversos processos, tais como floculação, velocidade de decantação e “scour lag”, e, também, a assimetria das correntes de maré (Lumborg *et al.*, 2003). A junção desses diversos processos torna difícil a previsão do transporte desses sedimentos (Teisson, 1991). Além disso, outro aspecto importante é a calibração e validação dos resultados, onde, muitas vezes acabam ocorrendo somente para os modelos hidrodinâmicos devido a dificuldade de se obter dados de campo. Apesar da calibração e validação conseguirem reproduzir a dinâmica da região de estudo, ainda podem ocorrer divergências entre o resultado modelado de sedimentos coesivos e o observado em campo, gerando incertezas quanto a capacidade de reprodução do modelo (Sun *et al.*, 2016).

No caso da Lagoa dos Patos, que é a região de interesse desse estudo, muitos são os estudos referentes a sua hidrodinâmica (Möller *et al.*, 2001; Castelão e Möller, 2003; Fernandes *et al.*, 2002, 2004; Marques *et al.*, 2010; Pagot *et al.*, 2007; Fassoni-Andrade *et al.*, 2015), contudo, pouco se sabe

sobre as concentrações de sedimento em suspensão (Hartmann, 1996; Marques *et al.*, 2010; Andrade-Neto *et al.*, 2012; Fassoni-Andrade *et al.*, 2016), mesmo esta informação sendo de extrema importância ambiental e econômica.

As crescentes concentrações de sedimento em suspensão transportadas dos rios para o interior da Lagoa dos Patos em função da erosão das suas margens e de cultivos extensivos, são preocupantes. Esse material é rico em sedimentos finos, que chegam à região costeira e eventualmente alimentam os bancos de lama ali existentes (Calliari *et al.*, 2009). Além disso, tais variáveis podem estar sujeitas aos efeitos dos eventos ENSO, os quais afetam os padrões de precipitação na região, e, por conseguinte, as variáveis hidrológicas. Nesse contexto, esse estudo pretende analisar a variabilidade espaço-temporal das concentrações de sedimento em suspensão da Lagoa dos Patos, visando contribuir para o entendimento e a previsão do comportamento dessa importante variável ambiental.

### **1.1. A Lagoa dos Patos**

Considerada a maior lagoa costeira do tipo estrangulado do mundo (Kjerfve, 1986), a Lagoa dos Patos (Figura 1) está localizada no extremo sul do Brasil e compreende uma área de 10.360 km<sup>2</sup> (Delaney, 1965). Apresenta profundidade média de 5 m (Möller *et al.*, 2001), podendo atingir até 16 m em seus canais dragados (Fernandes *et al.*, 2002).

Diversos autores (Möller *et al.*, 2001; Fernandes *et al.*, 2002; Vaz *et al.*, 2006; Marques *et al.*, 2010) apontam a ação dos ventos e as descargas fluviais como os principais mecanismos responsáveis pela dinâmica da lagoa. A maré astronômica (mista, com predominância diurna) apresenta amplitude reduzida (0.23 m) (Möller *et al.*, 2001) e pouca influência sobre a dinâmica desse ambiente, uma vez que seus efeitos são restritos ao canal de acesso do estuário (Fernandes *et al.*, 2004).

Os rios Guaíba e Camaquã, juntamente com o Canal São Gonçalo, são os principais tributários da Lagoa dos Patos (Figura 1A) e responsáveis pela drenagem hídrica de metade da área do RS (Castelão e Möller, 2003). Esses afluentes apresentam descarga média anual de 2.400 m<sup>3</sup>.s<sup>-1</sup> (Vaz *et al.*, 2006),

e se comportam como típicos rios de médias latitudes marcados por fortes variações sazonais: altas descargas no final do inverno e no início da primavera, e descargas moderadas no verão e outono (Möller *et al.*, 2001). Ainda, estão sujeitos aos ciclos El Niño/La Niña que afetam a região (Fernandes *et al.*, 2002), quando, em anos de El Niño, os valores de descarga podem atingir de 8.000 a 12.000 m<sup>3</sup>.s<sup>-1</sup> (Möller *et al.*, 1996).

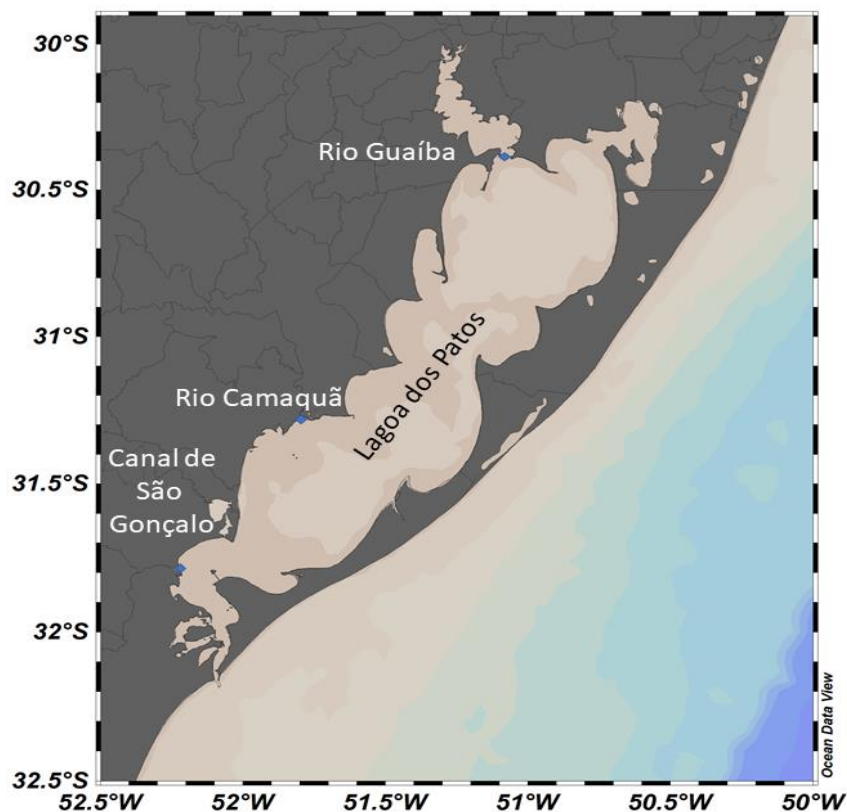


Figura 1 – Área de estudo. Os pontos azuis representam os principais afluentes da Lagoa dos Patos: Rio Guaíba (ao norte), Rio Camaquã (porção central) e Canal São Gonçalo (ao sul).

Durante períodos em que as descargas dos rios variam de baixas a moderadas ( $< 3.000 \text{ m}^3 \text{ s}^{-1}$ ), a ação do vento atua como principal mecanismo da circulação lagunar através da combinação da ação dos ventos local e remoto (Möller *et al.*, 2001). A predominância de ventos ao longo do ano é de direção nordeste, com inversões para ventos de oeste e sul devido as passagens de sistemas frontais (Möller *et al.*, 1996). De acordo com Castelão e Möller (2003) (Figura 2), durante a dominância do vento de NE (SO), ocorre um abaixamento (elevação) do nível na costa, favorecendo os fluxos em direção ao oceano (interior da lagoa).



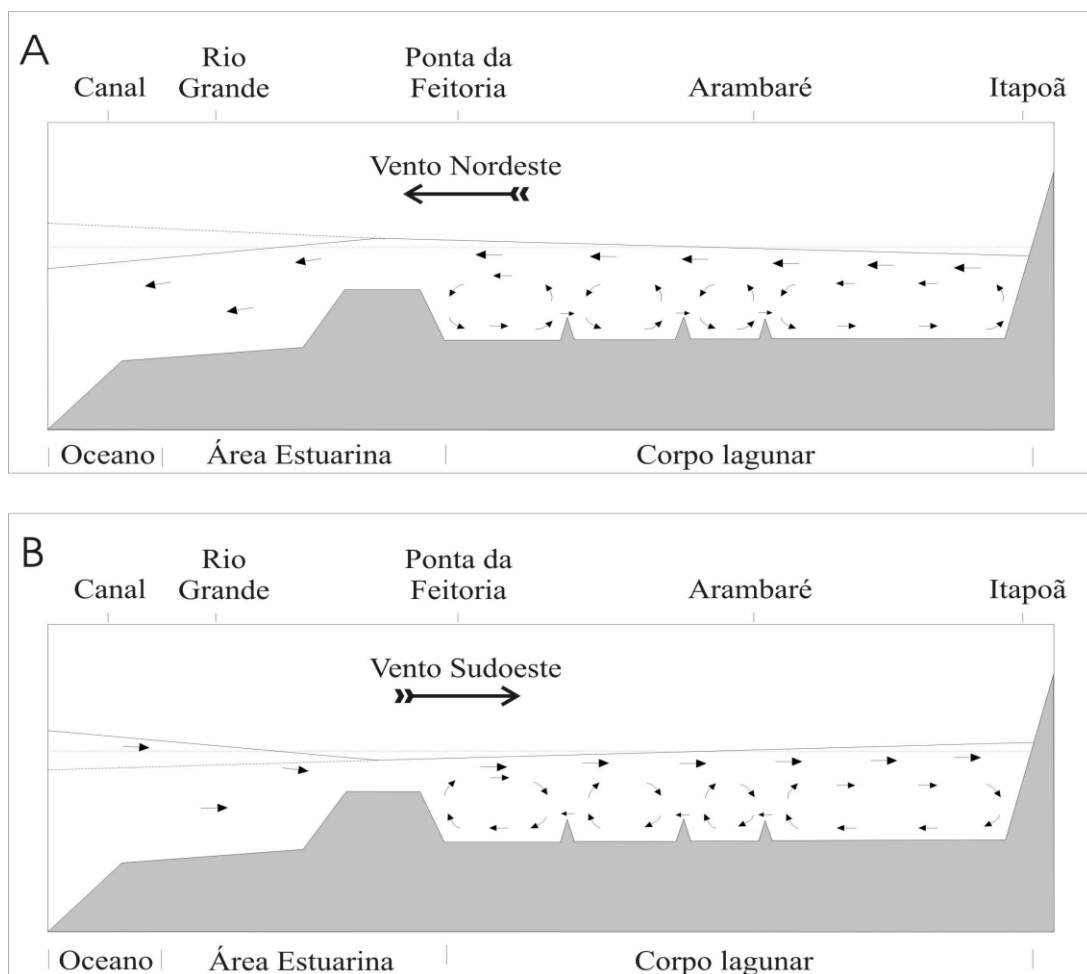


Figura 2 – Representação esquemática das ações dos ventos de (A) nordeste e (B) sudoeste na Lagoa dos Patos (Castelão e Möller, 2003).

Os sedimentos de fundo do corpo lagunar estão separados em (Figura 3A): areia e sedimentos mais grosseiros das margens até a isóbata de 5 m, e sedimentos finos (silte e argila) nas porções mais profundas (regiões centrais e canais) (Toldo Jr *et al.*, 2006). A respeito dos sedimentos em suspensão aportados pela descarga dos rios tributários e pelo processo de ressuspensão, Calliari *et al.* (2009) indicam o silte (80%) e a argila (15%) como os principais compostos presentes nesse ambiente, e ressaltam que as concentrações de silte (argila) diminuem (aumentam) no sentido do corpo lagunar até o estuário.

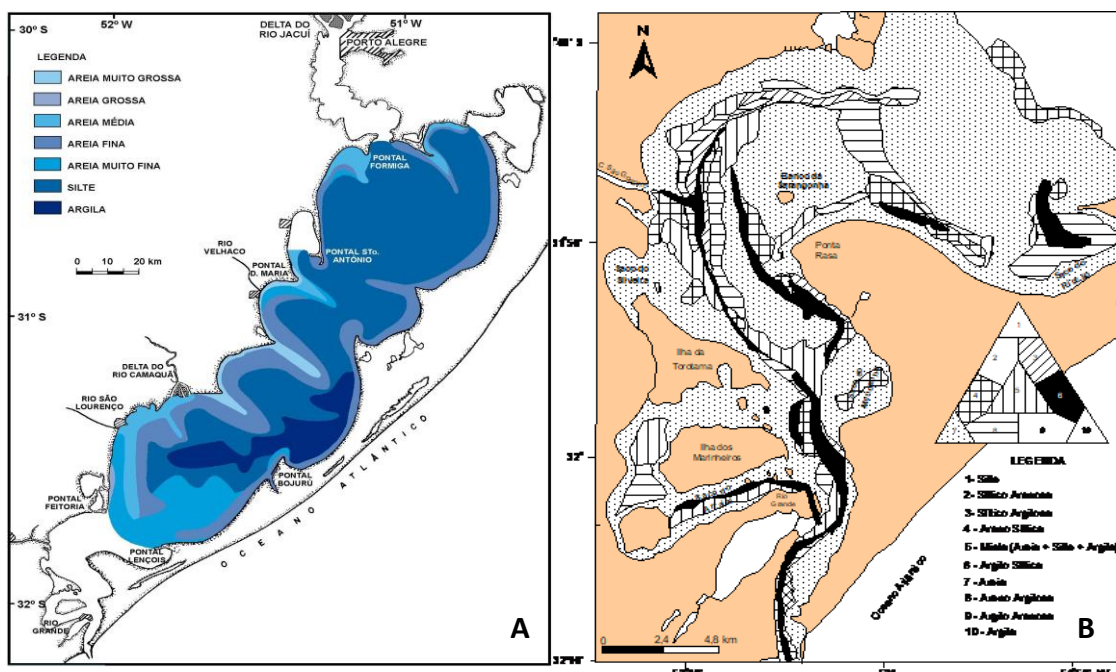


Figura 3 – A) Sedimentos de fundo do: A) corpo lagunar (Toldo Jr *et al*, 2006) e B) corpo estuarino (Calliari, 1980).

Na região estuarina, os sedimentos são provenientes da descarga fluvial dos rios Guaíba (ao norte) e Camaquã (porção central, traz sedimentos do escudo Sul-Rio Grandense), e do Canal de São Gonçalo (a sul, conexão Lagoa dos Patos – Lagoa Mirim), apresentando, então, grande variabilidade na composição dos sedimentos de fundo (Figura 3B) (Villwock, 1978; Hartmann e Rarkot, 1990). Em especial, os sedimentos oriundos do Canal de São Gonçalo, devido a sua localização e grande carga sedimentar, são os principais contribuintes para essa região (Hartmann e Rarkot, 1990). Além disso, essa região está sujeita as alterações morfológicas resultantes da transição entre a porção lagunar e a estuarina, nas quais a última ainda se encontra sujeita a influência do oceano adjacente e, por conta disso, a ação das ondas, a inserção de água salgada, a ação da flocculação e formação de zonas de turbidez máxima, o que pode ressuspender os sedimentos.

Nessa porção da Lagoa dos Patos, os sedimentos de fundo são mais finos (silte, argila e areia fina) (Calliari *et al.*, 2009) e seis desses tipos de sedimentos podem estar intimamente ligados a profundidade e níveis de energia da hidrodinâmica (Figura 3B). De forma geral, sedimentos como silte e

argila estão dispostos nas porções mais profundas e nas áreas rasas e protegidas.

# **Capítulo II:**

## Objetivos

## **2. OBJETIVOS**

### **2.1. Geral**

Analisar a variabilidade espaço-temporal das concentrações de sedimento em suspensão da Lagoa dos Patos através de técnicas de modelagem numérica.

### **2.2. Específicos**

- Avaliar a distribuição sazonal e interanual das concentrações de sedimento em suspensão na porção lagunar e estuarina;
- Avaliar a influência dos ciclos El Niño/La Niña no comportamento do sedimento em suspensão.

# **Capítulo III:**

## **Materiais e Métodos**

### 3.1. Modelo hidrodinâmico – TELEMAC-3D

O sistema Telemac foi desenvolvido pelo *Laboratoire National d'Hydraulique et Environnement* da companhia *Electricité de France* (EDF) e é composto por um conjunto de módulos tanto em 2D quanto em 3D abrangendo hidrodinâmica, transporte de sedimentos, ondas e qualidade da água. O modelo TELEMAC-3D é capaz de resolver as Equações de Navier-Stokes a partir da consideração da variação local da superfície livre do fluido, negligenciando o gradiente de densidade na equação da conservação de massa. Além disso, o modelo também considera a pressão hidrostática (Equação 1) e, para resolver a equação do movimento, aplica a aproximação de Boussinesq. Dessa forma, abaixo estão dispostas as seguintes equações: a Equação da Continuidade (Equação 2) e as Equações da Conservação do Momento resultantes (Equações 3, 4 e 5).

$$p = p_{atm} + \rho_0 g(\eta - z) + \rho_0 g \int_z^\eta \frac{\Delta\rho}{\rho_0} dz \quad (1)$$

$$\frac{\partial u}{\partial x} + \frac{\partial v}{\partial y} + \frac{\partial w}{\partial z} = 0 \quad (2)$$

$$\frac{\partial u}{\partial t} + u \frac{\partial u}{\partial x} + v \frac{\partial u}{\partial y} + w \frac{\partial u}{\partial z} = - \frac{1}{\rho} \frac{\partial p}{\partial x} + \nu \nabla^2 u + F_x \quad (3)$$

$$\frac{\partial v}{\partial t} + u \frac{\partial v}{\partial x} + v \frac{\partial v}{\partial y} + w \frac{\partial v}{\partial z} = - \frac{1}{\rho} \frac{\partial p}{\partial y} + \nu \nabla^2 v + F_y \quad (4)$$

$$\frac{\partial w}{\partial t} + u \frac{\partial w}{\partial x} + v \frac{\partial w}{\partial y} + w \frac{\partial w}{\partial z} = - \frac{1}{\rho} \frac{\partial p}{\partial z} - g + \nu \nabla^2 w + F_z \quad (5)$$

Onde: (u, v, w) são as componentes de velocidade dos eixos (x,y,z), respectivamente; p é a pressão em cada ponto do domínio;  $\nu$  é o coeficiente de viscosidade dinâmica;  $\nabla^2$  é o operador Laplaciano; ( $F_x$ ,  $F_y$ ,  $F_z$ ) representam os termos fontes, incluindo a força de Coriolis, a fricção de fundo e o arrasto de vento.

### 3.1.1. Fricção de Fundo

Na simulação hidrodinâmica, as forças da fricção de fundo (tensão de cisalhamento) atuam no sentido oposto ao deslocamento do fluido (velocidades de fundo) (Equação 6), o qual é fornecido pelo modelo de turbulência do TELEMAC-3D (Hervouet, 2007).

$$\vec{\tau} = -\mu \frac{\partial \vec{v}}{\partial \eta} \quad (6)$$

A partir da análise dimensional da tensão de cisalhamento de fundo, essa passa a ser expressa pela Equação 7.

$$\vec{\tau} = -\frac{1}{2} C_f \sqrt{u^2 + v^2} \quad (7)$$

Onde:  $C_f$  é o coeficiente adimensional de fricção; e  $\vec{V}$  é o campo de velocidade de fundo.

No modelo TELEMAC-3D existem algumas opções de coeficientes adimensionais de fricção, sendo elas: coeficiente de Chézy (Equação 8), Strickler (Equação 9), Manning (Equação 10) e Nikuradse (Equação 11). No presente estudo foi utilizado o coeficiente de Nikuradse.

$$C_h = 7.831 \ln\left(12 \frac{h}{k_s}\right) \quad (8)$$

$$C_s = \frac{2g}{h^{1/3} S^2} \quad (9)$$

$$C_m = \frac{2gm^2}{h^{1/3}} \quad (10)$$

$$C_n = 2gC_h^{-2} \quad (11)$$

Onde:  $g$  é a gravidade;  $h$  é a espessura da coluna;  $k_s$  é o tamanho do grão no fundo; e  $(C, S, m)$  são os respectivos coeficientes.

### 3.1.2. Cisalhamento do Vento



No modelo, a influência do vento é considerada no contorno superficial e a sua transferência de momento para a coluna de água acontece de forma similar à de fricção de fundo, sendo a sua parametrização baseada na lei quadrática da tensão da velocidade do vento. A importância de cada componente do vento na transferência de momento é expressa pelas Equações 12 e 13.

$$F_{wx} = \frac{1}{h} \frac{\rho_{ar}}{\rho} a_{vento} u_{vento} \sqrt{u_{vento}^2 + v_{vento}^2} \quad (12)$$

$$F_{wy} = \frac{1}{h} \frac{\rho_{ar}}{\rho} a_{vento} v_{vento} \sqrt{u_{vento}^2 + v_{vento}^2} \quad (13)$$

Onde:  $\rho_{ar}$  é a densidade do ar ( $1,029 \text{ kg.m}^{-3}$ );  $a_{vento}$  é o coeficiente adimensional de resistência do vento;  $(u_{vento}, v_{vento})$  são as componentes zonais e meridionais da velocidade do vento ( $\text{m.s}^{-1}$ ), respectivamente; e  $(F_{wx}, F_{wy})$  são as componentes zonais e meridionais da força de fricção do vento (N).

Dependente da rugosidade da superfície livre, da intensidade e pista de vento, a influência do vento torna-se um fenômeno complexo. Dessa forma, o coeficiente de influência do vento pode ser obtido de diversas formas. No modelo TELEMAC-3D, ele é obtido pela formulação abaixo, como proposta por Flather (1976).

$$\text{Se } |\overline{u_{vento}}| < 5 \text{ m.s}^{-1}, \text{ então } a_{vento} = 0,565 \cdot 10^{-3}$$

$$\text{Se } 5 < |\overline{u_{vento}}| < 19,22 \text{ m.s}^{-1}, \text{ então } a_{vento} = (-0,12 + 0,137 |\overline{u_{vento}}|) \cdot 10^{-3}$$

$$\text{Se } |\overline{u_{vento}}| > 19,22 \text{ m.s}^{-1}, \text{ então } a_{vento} = 2,513 \cdot 10^{-3}$$

### 3.1.3. Termo de Flutuabilidade

Nos termos  $F_x$  e  $F_y$  das equações horizontais de Navier-Stokes (Equações 3 e 4) estão incorporados os termos de flutuabilidade, os quais são oriundos da aplicação do termo de primeira ordem e representam as variações de densidade nas componentes de variações horizontais de pressão (Equações 14 e 15).

$$-\frac{1}{\rho} \frac{\partial p}{\partial x} \cong -\frac{1}{\rho_0} \left(1 - \frac{\Delta\rho}{\rho_0}\right) \frac{\partial p}{\partial x} \quad (14)$$

$$-\frac{1}{\rho} \frac{\partial p}{\partial y} \cong -\frac{1}{\rho_0} \left(1 - \frac{\Delta\rho}{\rho_0}\right) \frac{\partial p}{\partial y} \quad (15)$$

Assumindo a forma hidrostática (Equação 1), a aplicação da Equação da componente vertical de Navier-Stokes nas equações 14 e 15 resulta nos termos que representam as acelerações geradas pelas forças associadas aos escoamentos devido às variações de fluabilidade. Nas equações 16 e 17 estão expressos os termos barotrópico e baroclínico zonais e meridionais, respectivamente.

$$g \frac{\Delta\rho}{\rho_0} \frac{\partial \eta}{\partial x} - g \frac{\partial}{\partial x} \left( \int_z^\eta \frac{\Delta\rho}{\rho_0} dz \right) \quad (16)$$

$$g \frac{\Delta\rho}{\rho_0} \frac{\partial \eta}{\partial y} - g \frac{\partial}{\partial y} \left( \int_z^\eta \frac{\Delta\rho}{\rho_0} dz \right) \quad (17)$$

Ou seja, os termos de fluabilidade são originários do gradiente de pressão e estão incorporados nas variáveis  $F_x$  e  $F_y$  e a estimativa da densidade ( $\rho$ ) viabiliza o cálculo dos termos de fluabilidade.

#### 3.1.4. Transporte de Traçadores

O processo de transporte de traçadores no modelo TELEMAC-3D pode ser dividido em duas categorias: nos traçadores ativos (salinidade e a temperatura), que atuam alterando a densidade da água e o momento de inércia do fluxo; e os traçadores passivos, os quais não afetam a inércia e são meramente transportados. A evolução dos traçadores no domínio tridimensional é calculada pela equação 19.

$$\frac{\partial T}{\partial t} + u \frac{\partial T}{\partial x} + v \frac{\partial T}{\partial y} + w \frac{\partial T}{\partial z} = \nu_T \nabla^2 T + Q \quad (19)$$

Onde:  $T$  é o traçador ativo ou passivo;  $\nu_T$  é o coeficiente de difusão do traçador ( $\text{m}^2.\text{s}^{-1}$ );  $t$  é o tempo (s);  $(u, v, w)$  são os componentes da velocidade  $\vec{V}$  ( $\text{m}.\text{s}^{-1}$ ); e  $Q$  é a fonte ou sumidouro do traçador.

Para o transporte de sedimento em suspensão e processos relacionados (fluxos de erosão e deposição), o modelo TELEMAC - 3D resolve equações de advecção-difusão (Equação 20) para o transporte de um traçador ativo no sistema, determinando a evolução da sua concentração no tempo e no espaço. Dessa forma, foi adicionado o sedimento como terceiro traçador (além da temperatura e da salinidade) a fim de monitorar a sua evolução no tempo e no espaço.

$$\frac{\partial C}{\partial t} + u \frac{\partial C}{\partial x} + w \frac{\partial C}{\partial z} - u \frac{\partial (W_c C)}{\partial x} = \frac{\partial}{\partial x} \left( K_x \frac{\partial C}{\partial x} \right) + \frac{\partial}{\partial y} \left( K_y \frac{\partial C}{\partial y} \right) + \frac{\partial}{\partial z} \left( K_z \frac{\partial C}{\partial z} \right) \quad (20)$$

Onde: (u,w) representam as velocidades do fluido (m.s<sup>-1</sup>); C é a concentração do sedimento em suspensão (kg.m<sup>-3</sup>); W<sub>c</sub> é a velocidade de decantação do sedimento em suspensão (m<sup>2</sup>.s<sup>-1</sup>); (K<sub>x</sub>,K<sub>y</sub>,K<sub>z</sub>) são os coeficientes de difusão turbulenta do sedimento (m<sup>2</sup>.s<sup>-1</sup>).

Ademais, a velocidade de deposição desses sedimentos em suspensão utilizada pelo modelo considera os efeitos de turbulência e da concentração para deposição dos sedimentos, o que é de suma importância para a formação de flocos, formadas pelas colisões entre as partículas, e para a sua quebra intensificadas pelos movimentos turbulentos, e a flocculação também foi considerada no transporte. A equação utilizada para o cálculo da velocidade de deposição dos sedimentos em suspensos (Equação 21) segue a teoria de Van Leussen (1994).

$$W_s = k_1 C^{m_1} \frac{1 + aG}{1 + bG^2} \quad (21)$$

$$G = \sqrt{\frac{\varepsilon}{\nu}} \quad (22)$$

Onde: k<sub>1</sub> e m<sub>1</sub> são constantes empíricas; C é a concentração de sedimentos ao longo da coluna d'água; a é o coeficiente referente a flocculação; b é o coeficiente referente à destruição do floco; ν é o coeficiente de viscosidade turbulenta; G é o gradiente de velocidade absoluto, e ε é a taxa de dissipação. Para a e b foram utilizados 0.3 e 0.09, respectivamente, de acordo com Van Leussen (1994).

A classe do sedimento em suspensão simulada é o silte, como já utilizado por Marques *et al.* (2010) para o mesmo ambiente. Foram realizadas simulações nos períodos de 2002 a 2006 que, apesar do curto espaço de tempo, são caracterizados pela incidência de ciclos completos de eventos ENSO.

### 3.2. Malha batimétrica

O domínio foi discretizado através de uma malha (Figura 4) baseada na técnica de Elementos Finitos, na qual a mesma é composta por elementos triangulares, os quais permitem uma melhor ilustração das características batimétricas e morfológicas do ambiente, além de otimizar a simulação pela possibilidade de utilizar refinamentos diferenciados.

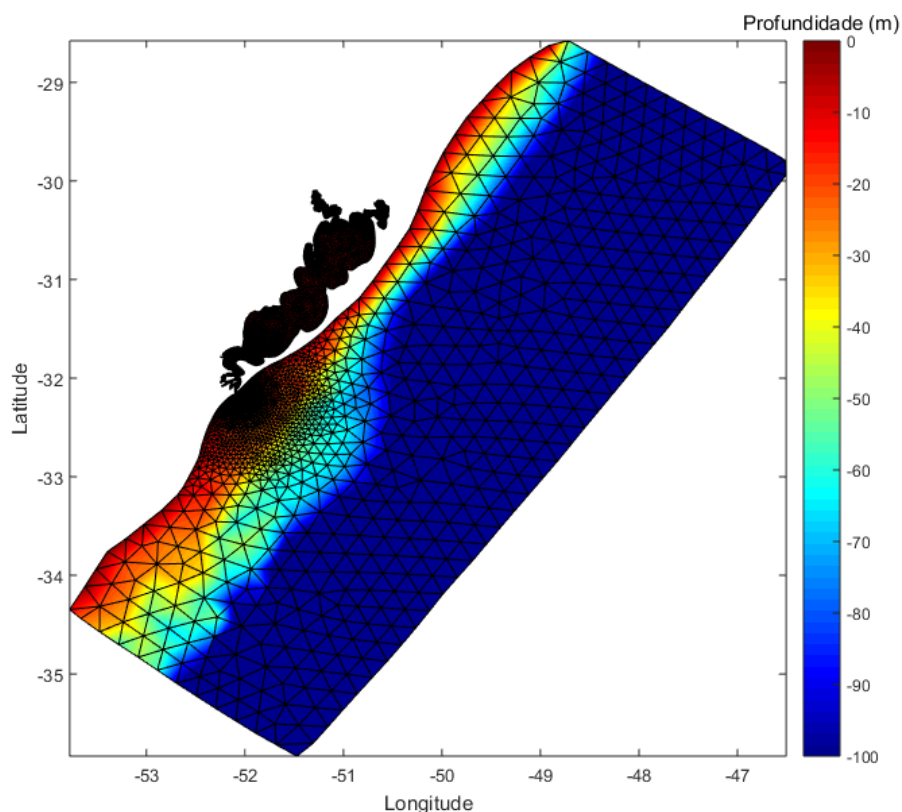


Figura 4 – Malha batimétrica.

A malha utilizada abrange o domínio entre 28°- 36°S e 46°- 54°W, e foi gerada através do Software BlueKenue ([http://www.nrc-cnrc.gc.ca/eng/solutions/advisory/blue\\_kenue\\_index.html](http://www.nrc-cnrc.gc.ca/eng/solutions/advisory/blue_kenue_index.html)), através do uso dos dados batimétricos digitalizados de cartas náuticas da Diretoria de Hidrografia e Navegação (DHN), e complementados com os dados disponibilizados pela

Superintendência do Porto do Rio Grande (SUPRG). A malha resultante é composta por cerca de 32.943 elementos, 17.770 nós, sete níveis sigma e sua profundidade se estende até 3300 m.

### 3.3. Condições iniciais e de contorno

#### 3.3.1. Fronteiras oceânicas

Os dados de altura da superfície do mar do OSU *Tidal Inversion System* (OTIS - Edgbert e Erofeeva, 2002), prescrevendo a elevação da superfície e a velocidade de corrente de maré regional, e campos de salinidade (Figura 5) e temperatura, obtidos através do projeto HYCOM + NCODA Global (*HYbrid Coordinate Ocean Model*, <https://hycom.org/>), com resolução espacial e temporal de  $1/12^\circ$  e 3h, respectivamente, foram utilizados nas fronteiras oceânicas.

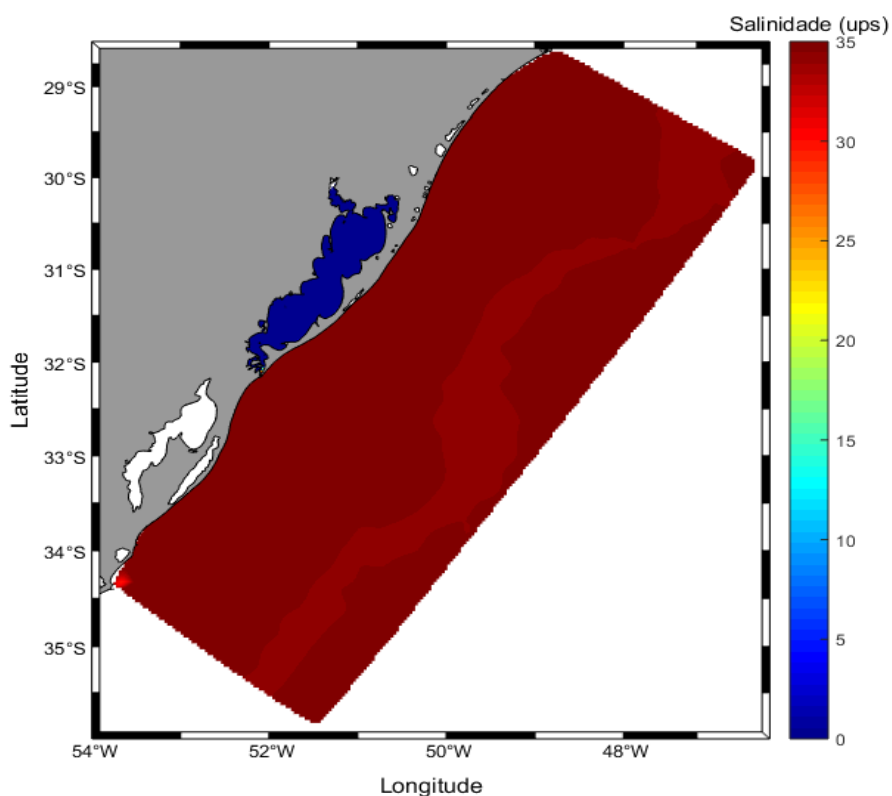


Figura 5 – Campo inicial de salinidade para todo o domínio.

#### 3.3.2. Fronteiras superficiais

As fronteiras superficiais do domínio foram forçadas com os dados de 6/6h de vento (Figura 6) e resolução espacial de  $0.75^\circ$  do ECMWF (*European Center*

for *Medium-Range Weather Forecast*, <http://www.ecmwf.int/>) interpolados espacial e temporalmente para cada ponto da malha numérica, e para cada passo de tempo.

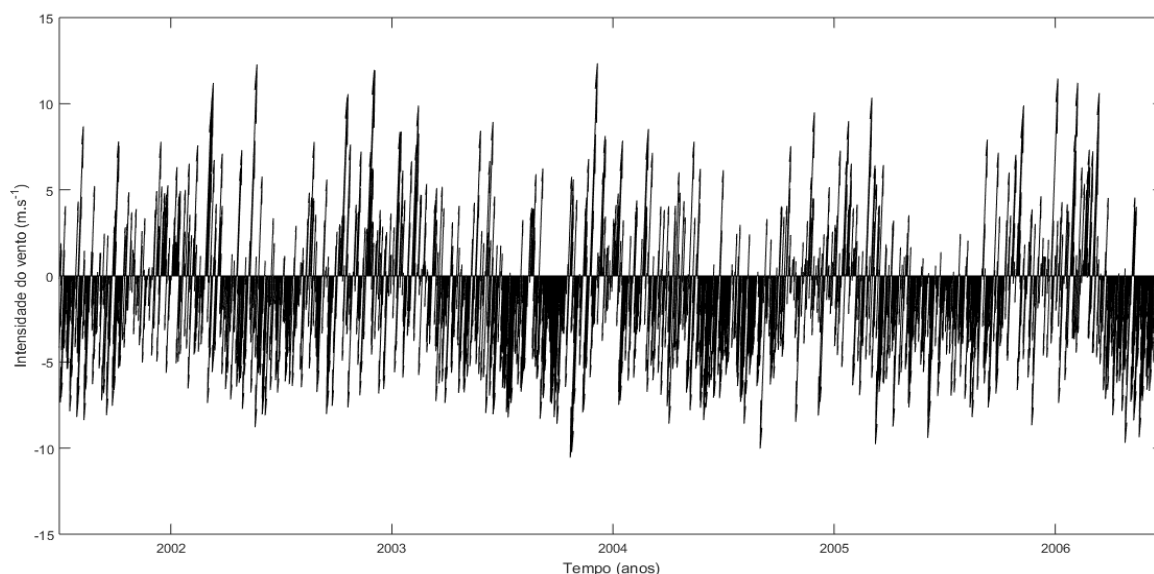


Figura 6 - Série temporal de intensidade do vento para o período estudado.

### 3.3.3. Fronteiras continentais

Para as fronteiras continentais, dados diários (Figura 7) de vazão do Rio Guaíba e Rio Camaquã foram obtidos junto à Agência Nacional das Águas (ANA, <http://www.ana.gov.br>). Para os dados do Canal São Gonçalo foram utilizados dados de nível obtidos através da Agência da Lagoa Mirim (ALM, <https://wp.ufpel.edu.br/alm/>) e transformados em dados diários de vazão a partir da curva-chave (Oliveira *et al.*, 2015). Para as condições iniciais da concentração do sedimento em suspensão dos tributários foram utilizados os seguintes valores: 200 mg.L<sup>-1</sup>, 100 mg.L<sup>-1</sup> e 150 mg.L<sup>-1</sup> (Hartmann e Rarkot, 1990) para o rio Guaíba, rio Camaquã e Canal São Gonçalo, respectivamente.

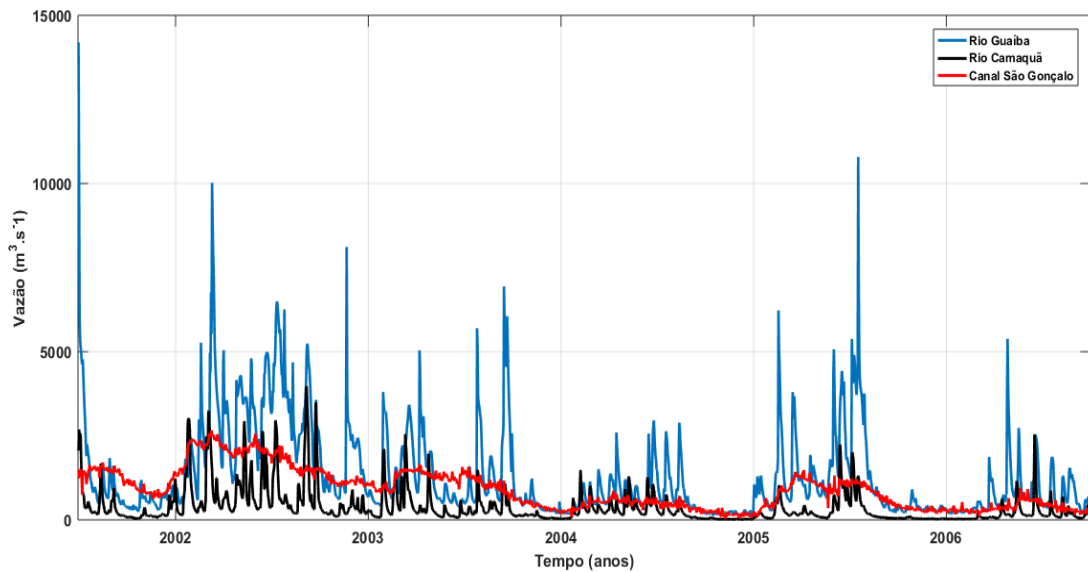


Figura 7 – Série temporal da vazão do Rio Guaíba, Rio Camaquã e Canal São Gonçalo para o período estudado (2002-2006).

### 3.4. Calibração e Validação do modelo

O exercício de calibração tem o intuito de otimizar os valores dos principais parâmetros físicos do modelo, visando a reprodução das condições observadas no ambiente. Como proposto por Fernandes *et al.* (2001; 2002) e Marques *et al.* (2010), os procedimentos de calibração e validação do modelo para a referida área de estudo foram feitos a partir da comparação estatística (Walstra *et al.*, 2001) entre o uso de dados coletados em campo e dos dados modelados.

O exercício de calibração e validação deste trabalho foi realizado com base nos dados de salinidade, velocidade de corrente e CSS medidos para os meses de janeiro de 2006. Os dados de salinidade e velocidade de corrente foram obtidos, respectivamente, por um CT e um ADCP próximo a praticagem de Rio Grande (Figura 1, P2 – manuscrito). Os dados de CSS foram obtidos pela DMAE (Departamento Municipal de Água e Esgoto), os procedimentos de aquisição e processamento de CSS é apresentado por Andrade Neto *et al.*, (2012).

Os resultados da calibração e validação serão descritos no capítulo IV.

### 3.5. Dados Climáticos e de Precipitação

Para identificar a relação entre CSS e a variabilidade climática, dados mensais do Southern Oscillation Index (SOI) foram obtidos a partir da Earth

System Research Laboratory (<https://www.esrl.noaa.gov/psd/enso/soi>). Além disso, dados diários de precipitação foram obtidos e convertidos em médias mensais e extraídas séries temporais na boca do rio Guaíba (Figura 1A); esses dados foram adquiridos através da Global Precipitation Climate Centre (GPCP, <https://www.dwd.de/EN/ourservices/gpcc/gpcc.html>)

### **3.6. Variabilidade temporal**

As séries temporais de concentração de sedimento em suspensão apresentam diversos sinais de fenômenos oscilatórios, o que torna necessário o uso de uma análise espectral. Portanto, para avaliar o padrão de variabilidade da série temporal de concentração de sedimento em suspensão foi utilizada a transformada de ondaletas, a qual fornece informações em diferentes domínios de frequência e também do tempo de acordo com a escala a ser analisada através da translação de uma ondaleta original (Torrence & Compo, 1998).



# Capítulo IV:

## Resultados e Discussões

**P**ara a obtenção do título de Mestre pelo Programa de Pós-Graduação em Oceanografia Física, Química e Geológica, é requerido que o discente realize a submissão de pelo menos um artigo científico como primeiro autor em periódico com corpo indexado. Desse modo, os resultados da pesquisa desenvolvida durante o período de mestrado e a discussão dos resultados serão apresentados em forma de artigo neste Capítulo. O manuscrito, de autoria de Liliane Paranhos Bitencourt, Elisa Helena Fernandes e Pablo Dias da Silva, é intitulado “**Spatio-temporal variability of suspended sediment concentration on a shallow and turbid lagoon**” e foi submetido para publicação no periódico “*Water Resources Research*”.

## **Spatio-temporal variability of suspended sediment concentration on a shallow and turbid lagoon**

Liliane Paranhos Bitencourt<sup>1\*</sup>, Elisa Helena Fernandes<sup>1</sup>, Pablo Dias da Silva<sup>1</sup>

<sup>1</sup> Instituto de Oceanografia, Universidade Federal do Rio Grande, Rio Grande, RS, Brazil.

\*Corresponding author:

E-mail address: liparanhosb@gmail.com

### **1. Introduction**

Coastal lagoons and estuaries are highly complex and dynamic coastal systems. They are marked by high concentrations of suspended sediment from river discharge, erosion and/or seabed resuspension (Lihan *et al.*, 2008; Ruhl and Schoellhamer, 2004). Suspended sediment concentrations (SSC) in water play a significant role in determining the water quality of these systems due to its capacity of aggregating and transporting poorly water-soluble pollutants (Etemad-Shahidi *et al.*, 2010).

SSC are relevant to biogeochemical cycling, affecting light penetration in the water column, and consequently, primary production (Miller and McKee, 2004; Lopes *et al.*, 2006). Another important aspect is the key role of high SSC as sediment supply to adjacent coastal regions since continental waters have higher SSC than the oceans (Milliman and Meade, 1983). Furthermore, they affect sedimentation rates on navigational channels and ports (Horowitz, 2003).

Hence, it is necessary to understand and monitor the distribution and spatio-temporal variability of suspended sediments in coastal environments (Dogliotti *et al.*, 2016). Traditional field sampling methods, however, are expensive and space-time limited (Vantrepotte *et al.*, 2011), making numerical modelling a suitable tool for this purpose. Despite its complexity, numerical modelling experiments are cheaper to execute, provide wide space-time coverage, and can focus on areas of interest.

Furthermore, modelling the SSC of cohesive sediments can be important to estimate several aspects related to the effects of the discharge of environmental pollutants, dredging and disposal materials in ports, and

optimization of dredging operations based on the understanding of sediment erosion, transport and deposition zones in different spatio-temporal scales (Lumborg *et al.*, 2003).

Several studies using numerical modelling data to understand and describe the distribution and dynamics of SSC have been conducted worldwide (Villaret and Trowbridge, 1991; Lumborg *et al.*, 2003; 2005; Wang *et al.*, 2007; Marques *et al.*, 2010; Silva *et al.*, 2015; Krajewski *et al.*, 2017; Santoro *et al.*, 2017). However, modelling of cohesive suspended sediments had mainly been studied in small time-scales, which do not allow identifying longer variability patterns.

Along with the La Plata River, Patos Lagoon is an important contributor of sediment to the continental shelf in south Brazil. The Patos Lagoon drains half of the Rio Grande do Sul state, and continental contributions get to the system through the main tributaries (Guaíba and Camaquã rivers and São Gonçalo Channel, Figure 1) transporting SSC throughout the lagoon. While coarser sediments in suspension tend to deposit in regions of low hydrodynamics inside the lagoon, fine sediments in suspension are carried further towards the coast. Furthermore, recent studies suggested that SSC are increasing in the Patos Lagoon due to climate change effects. Besides water quality aspects and its effects in the biota (Garcia *et al.*, 2003; Moller *et al.*, 2009; Seiler *et al.*, 2015), the increasing SSC is of environmental concern and interest as this material is related to harbour siltation and feeds the mud deposits off Cassino Beach (Calliari *et al.*, 2009).

The Patos Lagoon hydrodynamics was studied by several authors using in situ data (Möller *et al.*, 2001; Castelão and Möller, 2003), numerical modelling (Fernandes *et al.*, 2002, 2004; Marques *et al.*, 2010), and remote sensing (Pagot *et al.*, 2007; Fassoni-Andrade *et al.*, 2016), but just a few of them focus on the SSC. Previous studies are restricted to local scales (Hartmann, 1996; Marques *et al.*, 2010; Andrade-Neto, 2011), and just a few studied the entire lagoon (Seiler *et al.*, 2015; Fassoni-Andrade *et al.*, 2015) because of the difficulty in systematically sample this large water body (240 km long). Thus,

apart from its considerable environmental and economic importance, the SSC variability in the Patos Lagoon is still poorly understood.

Previous studies have recognized ENSO events impacts on rivers discharge pattern (Vaz *et al.*, 2004), winds (Möller *et al.*, 2001; 2009), estuarine circulation (Fernandes *et al.*, 2002), and biota (Garcia *et al.*, 2003; Moller *et al.*, 2009), mainly due to ENSO changes on atmospheric conditions. During El Niño (La Niña) events, the precipitation rates are higher (lower) than the mean, directly affecting freshwater discharges contributions at northern Patos Lagoon (Moller *et al.*, 2009) and variables related to it (Fernandes *et al.*, 2002). However, its effects on the interannual variability of SSC in this area are also poorly understood.

Therefore, the aim of this study is to evaluate the spatio-temporal variability of the SSC at the Patos Lagoon based on numerical modelling experiments, and its relation to climate variability. For this purpose, five years (2002-2006) of high-resolution hydrodynamic + SSC simulations were carried out with the TELEMAC-3D Model. Data and methods are described in Section 2, and results and discussion related to: (i) description of spatio-temporal suspended sediment patterns, (ii) suspended sediment behaviour at the estuarine area; (iii) suspended sediment variability, were explored in Section 3. Finally, conclusions are presented in Section 4.

## **2. Data and Methods**

### **2.1. Study area**

With a length of 240 km, NE-SW orientation, an average width of 40 km and a surface area of 10,360 km<sup>2</sup>, the Patos Lagoon (Figure 1) is the largest choked coastal lagoon in the world (Kjerfve, 1986). It is an extensive and shallow (5 m mean depth) lagoon, located in the southernmost part of Brazil. The lagoon is connected to the Atlantic Ocean through a single narrow channel (Möller *et al.*, 2001). The water and suspended matter exchanges between the lagoon and its adjacent ocean set up physical-chemical characteristics that control ecological processes, and species habits and development (Seeliger, 2001).

Several authors highlighted the importance of winds and freshwater discharge on the Patos Lagoon dynamics (Möller *et al.*, 2001; Fernandes *et al.*,

2002; Vaz *et al.*, 2006; Marques *et al.*, 2010). Tides (mixed, diurnal dominance) are microtidal with reduced mean amplitude (0.23 m) (Möller *et al.*, 2001), being restricted to the coast and lower estuarine zone (Fernandes *et al.*, 2004; Marques *et al.*, 2010).

The Guaíba river, Camaquã river, and São Gonçalo channel are the main lagoon's tributaries, with a total mean annual discharge of  $2,400 \text{ m}^3 \cdot \text{s}^{-1}$  (Vaz *et al.*, 2004), exhibiting a mid-latitude discharge pattern with strong seasonal variations: higher discharges over latter winter and earlier spring, and moderate discharges during summer and fall (Moller *et al.*, 2001). Moreover, ENSO events affect this region (Fernandes *et al.*, 2002), and result in higher (El Niño) or lower (La Niña) freshwater discharges. During El Niño periods the lagoon can reach peaks of  $8,000$  and  $12,000 \text{ m}^3 \cdot \text{s}^{-1}$  (Moller *et al.*, 1996). When the river discharge is above  $3,000 \text{ m}^3 \cdot \text{s}^{-1}$ , it controls the Patos Lagoon hydrodynamics (Moller *et al.*, 2001), substantially blocking the seawater intrusion within the lagoon (Fernandes *et al.*, 2002).

On the other hand, according to Moller *et al.* (2001) and Castelão and Moller (2003), the lagoon dynamics is controlled by winds (local and remote) in periods of low to moderate freshwater discharges. In this area, there is an alternation of winds from NE to S-SW on a scale of days due to the passage of cold fronts (Moller *et al.*, 1996). Nevertheless, NE winds dominate throughout the year (Moller *et al.*, 2001). Castelão and Moller (2003) reported that during NE (SW) wind dominance, there is a depression (elevation) in coastal sea surface, resulting in seaward (landward) flows between the lagoon and the coast.

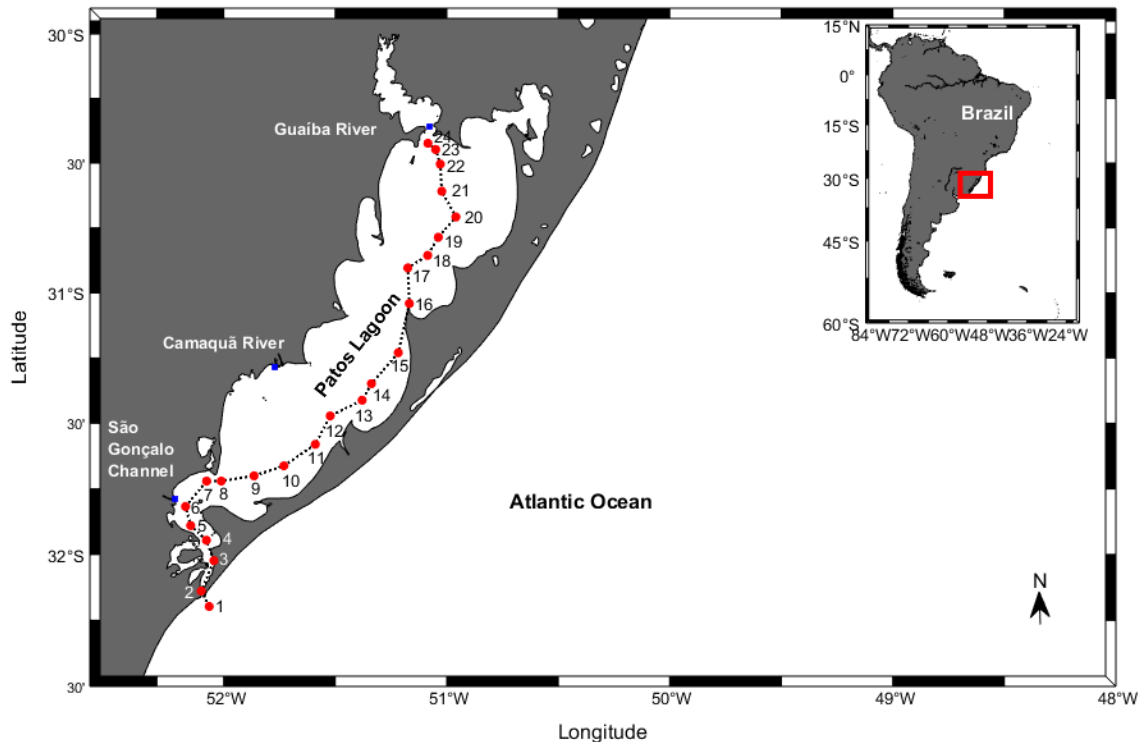


Figure 1 - Study area. Blue dots show the geographic position of Patos Lagoon major tributaries, and red dots represent points from where model results were extracted in the study area (Figure 7).

The morphological and sedimentological features of the Patos Lagoon have been described by Toldo Jr *et al.* (2006), and Calliari *et al.* (2009). The bottom sediments are distributed as: 1) sandy and narrow sediments in the lagoon's margins (5 m isobath); and 2) muddy sediments (silt and clay) in deeper portions (central regions and channels). Silt (80%) and clay (15%) are the main sediment types observed in suspension in the Patos Lagoon and they come from river and resuspension processes (Toldo Jr *et al.*, 2006). Calliari *et al.* (2009) pointed out that silt (clay) concentration decreases (increases) towards to estuary.

## 2.2. Field Data

The dataset used for the model calibration and validation (Section 2.2.3 and Section 3.1) was obtained in January 2006 in the Patos Lagoon. Current velocity data was obtained by a 1000 Hz Sontek ADP (Acoustic Doppler Profiler) with a temporal resolution of 1h, moored at Praticagem Station (13 m depth, P2, Figure 1). Salinity data was obtained by CTs moored at 1 and 10 m at the Naval Station (Figure 1), with a temporal resolution of 1h. SSC data was

obtained by the DMAE (Water and Sewage Municipal Department) at the Guaíba River mouth (Figure 1), with a temporal resolution of 24h. Andrade Neto *et al.* (2012) presents the data acquisition and processing.

### 2.3. Numerical Model

#### 2.3.1. TELEMAC Model

The TELEMAC System (<http://www.opentelemac.org/>, EDF) includes 2D and 3D modules, solving the 3D Reynolds-Averaged Navier-Stokes equations, considering the Boussinesq and hydrostatic approximations (Hervouet, 2007; Villaret *et al.*, 2013), aiming to obtain a more accurate representation of simulations in regions with accentuated bathymetric gradients and complex morphology. The model is based on the finite element technique, allowing selective refinement of the numerical mesh at key locations in the domain and boundary fitting (sigma transformation) for vertical discretisation (Bedri *et al.*, 2013).

Regarding the suspended sediment transport processes, the TELEMAC-3D model solves the mass conservation equation, which simulates the temporal and spatial variations of active tracers, such as salinity, temperature, and suspended sediment (Equation 1). Also, erosion and deposition rates are presented in Equations 2 and 3, respectively.

$$\frac{\partial C}{\partial t} + u \frac{\partial C}{\partial y} + w \frac{\partial C}{\partial z} - u \frac{\partial (W_c C)}{\partial y} = \frac{\partial}{\partial x} \left( K_x \frac{\partial C}{\partial x} \right) + \frac{\partial}{\partial y} \left( K_y \frac{\partial C}{\partial y} \right) + \frac{\partial}{\partial z} \left( K_z \frac{\partial C}{\partial z} \right) \quad (1)$$

$$F_{erosion} (kg/m^2.s) = M \left( \frac{\tau_b}{\tau_{ce}} - 1 \right) \quad (2)$$

$$F_{deposition} (kg/m^2.s) = P_d W_c C \quad (3)$$

Where: (u,w) represent fluid velocities (m.s<sup>-1</sup>); C is the concentration of suspended sediment (kg.m<sup>-3</sup>); W<sub>c</sub> is suspended sediment settling velocity (m<sup>2</sup>.s<sup>-1</sup>); (K<sub>x</sub>,K<sub>y</sub>,K<sub>z</sub>) are coefficients of turbulent sediment diffusion (m<sup>2</sup>.s<sup>-1</sup>); M is sediment coefficient; τ<sub>b</sub> and τ<sub>ce</sub> are bottom shear stress (N/m<sup>2</sup>) and critical erosion stress (N/m<sup>2</sup>), respectively; P<sub>d</sub> is the probability of deposition; F<sub>erosion</sub> is the erosion rate (kg/m<sup>2</sup>.s) and F<sub>deposition</sub> is the deposition rate (kg/m<sup>2</sup>.s).

The suspended sediment class used in this study was fine silt (Marques *et al.*, 2010), and a simulation for the period between 2002 and 2006 was carried out based on the identification of a clear ENSO cycle.

### 2.3.2. Numerical Mesh

The model domain (Figure 2) was represented by a finite element mesh based on digitalized nautical charts of bathymetric data obtained from the Brazilian Navy and complementary data provided by the Port of Rio Grande Administration (SUPRG). The domain covers from 28° - 36°S to 46° - 54°W and reaches 3.300 m depth. The grid consists of 32.943 elements, 17.770 nodes and 7 sigma levels irregularly distributed, i.e., 0.00, 0.10, 0.20, 0.50, 0.70, 0.90, 1.00.

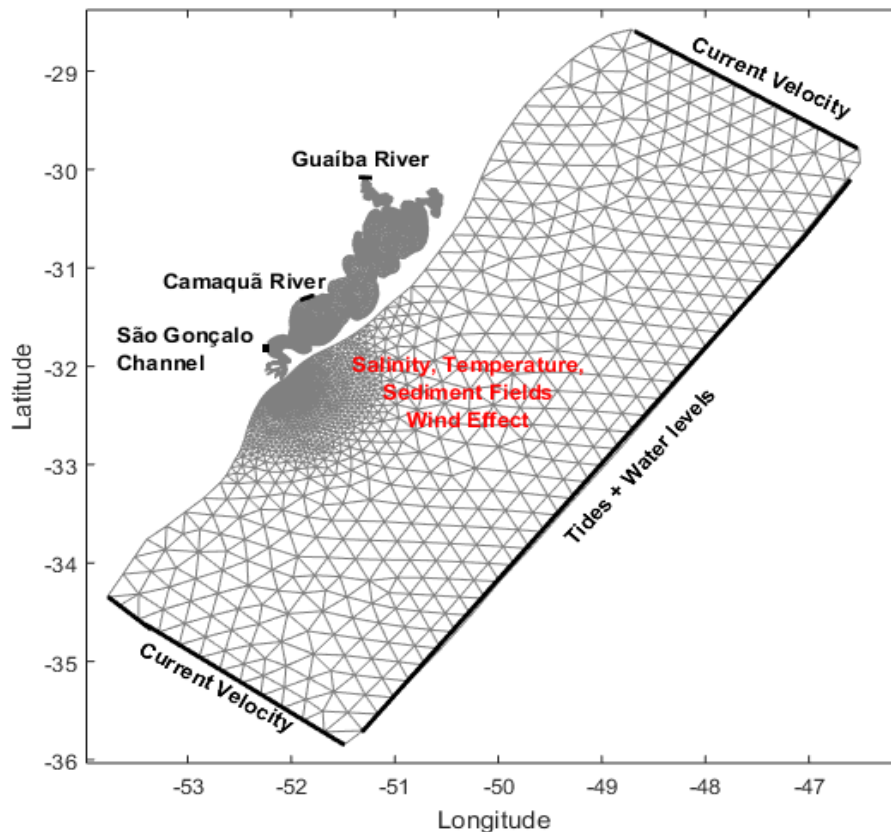


Figure 2 – Numerical mesh of the model domain and identification of initial and boundary conditions for the TELEMAC-3D model.

### 2.3.3. Initial and Boundary Conditions



Figure 2 summarizes the localization and type of the initial and boundary conditions considered in this numerical experiment. In the oceanic boundary were used: (i) elevations and regional tide velocity fields obtained by OSU Tidal Inversion System (OTIS – Edgbert & Erofeeva, 2002), internally coupled (TPXO) to TELEMAC; and (ii) temperature and salinity fields from HYCOM + NCODA Global (*HYbrid Coordinate Ocean Model*, <https://hycom.org/>) Project, with temporal and spatial resolution of 3h and 0.08°, respectively.

In the superficial boundary was used ECMWF (*European Center for Medium-Range Weather Forecast*, <http://www.ecmwf.int/>) ERA-Interim wind data with 6h and 0.75° temporal and spatial resolution, respectively. This data is interpolated in time and space for every point of the numerical mesh.

In the continental boundary, daily river discharge data from the main tributaries (Guaíba and Camaquã Rivers) were provided by the Brazilian National Water Agency (ANA, [www.hidroweb.ana.gov.br](http://www.hidroweb.ana.gov.br)). For the São Gonçalo Channel, water level values were obtained from the Mirim Lagoon Agency (ALM, <https://wp.ufpel.edu.br/alm/>) and converted into daily freshwater discharges based on the Oliveira *et al.* (2015) rating curve method. The river boundaries SSC were considered constant due to the lack of measurements and were assigned values of 200 mg.L<sup>-1</sup>, 100 mg.L<sup>-1</sup>, and 150 mg.L<sup>-1</sup> to Guaíba River, Camaquã River, and São Gonçalo Channel, respectively.

#### 2.4. Calibration and Validation

The model calibration and validation consist of comparisons between model results and in situ data for the same period and location, which are quantified based on statistical analysis (RMAE and RMSE) (Fernandes *et al.*, 2001; 2002; Marques *et al.*; 2010). In this study, the calibration and validation period covered from 1 to 30 of January 2006, and different variables were analysed in each process. The model's performance will be classified according to Walstra *et al.* (2001) (Table 1).

Table 1 - Classification of errors (Walstra *et al.*, 2001).

Qualification	Excellent	Good	Reasonable/fair	Poor	Bad
RMAE	<0.2	0.2 - 0.4	0.4 – 0.7	0.7 – 1.0	>1.0

For the calibration exercise, time series of surface and bottom current velocity were extracted and compared to in situ current velocity data (Section 2.1). Furthermore, time series of SSC data were extracted from the model and compared to in situ SSC data at Guaíba River. In the validation exercise, time series of surface and bottom salinity were compared to the corresponding in situ data.

Figure 3 illustrates the temporal evolution of modelling results (black) and in situ (red) time series of current velocity at the surface (Figure 3a) and bottom (Figure 3b) as the best result obtained in the model calibration. Table 2 presents the best set of physical parameters used in this experiment. In both surface (Figure 3a) and bottom (Figure 3b) current velocity time series, the model reproduced the trend of in situ data for the Patos Lagoon. The model reproduction is classified as good according to Walstra *et al.* (2001) (Table 1), with RMAE= 0.2382 and RMAE= 0.2834 at the surface and bottom, respectively. RMSE values ranged between 0.3642 and 0.3984 m.s<sup>-1</sup>. Measured and calculated comparison of SSC time series at the Guaíba River (Figure 3c) for the same period shows an excellent model reproduction (RMAE=0.0241). The RMSE value was nearly 4.41 mg.L<sup>-1</sup>.

Table 2 – Best set of physical parameters used in the calibration exercise.

<i>Parameters</i>	
Timestep	60 s
Coriolis	-7.70 x 10 <sup>-5</sup> N.m <sup>-1</sup> .s <sup>-1</sup>
Horizontal turbulence model	Smagorinski
Vertical turbulence model	Mixing length
Mixing length scale	10 m
Law of bottom friction	Nikuradse
Coefficient of wind influence	3 x10 <sup>-6</sup> N.m <sup>-1</sup> .s <sup>-1</sup>
Sediment settling velocity	Van Leussen
Critical shear stress for deposition	0.01 N.m <sup>-2</sup>
Critical erosion shear stress of the mud layers	1.5 N.m <sup>-2</sup>
Suspended sediment class	Fine silt

Based on the best set of physical parameters from the calibration experiment, a validation exercise was carried out for salinity time series at the surface (Figure 3d) and at the bottom (Figure 3e). The model reproduction

(black line) of measured salinity (red line) at the surface and bottom was classified as excellent, with RMAE of 0.1971 and 0.0357, respectively. RMSE values ranged from 4.5549 to 7.7387 psu.

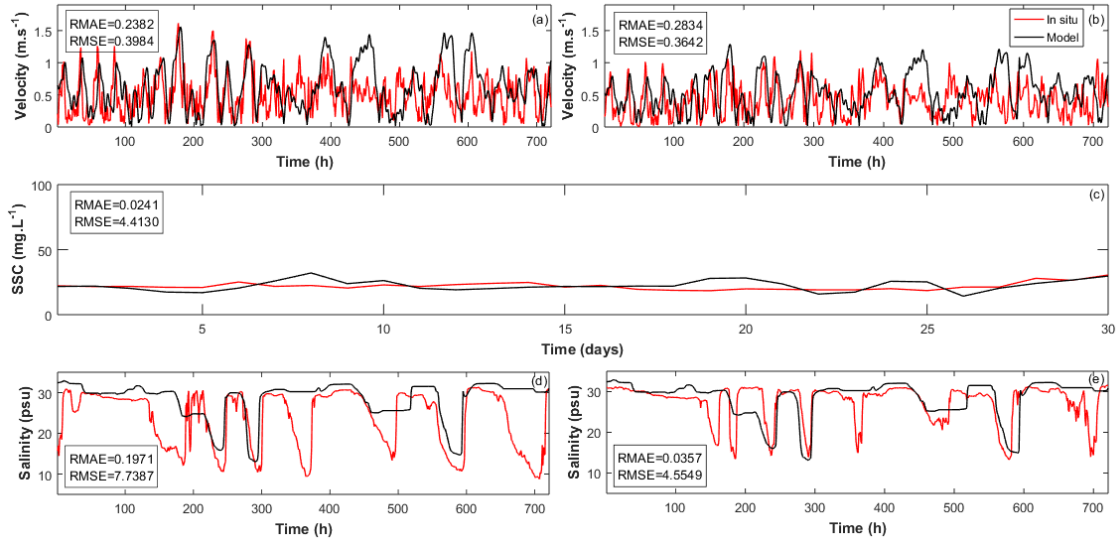


Figure 3 - Comparison between in situ (red) and model (black) data of: (a) surface and (b) bottom velocities; (c) SSC at Guaíba River; (d) surface and (e) bottom salinities for January 2006.

## 2.5. Climate and precipitation data

In order to identify the relation between SSC and large-scale climate variability, monthly Southern Oscillation Index (SOI) values were obtained from the Earth System Research Laboratory (<https://www.esrl.noaa.gov/psd/enso/soi>). SOI is a standardized index based on sea level pressure differences between Tahiti and Darwin, Australia. SOI is positive (negative) when La Niña (El Niño) phase is detected. Yet, its magnitude determines the events intensity.

Daily precipitation data for the Guaíba river mouth (Figure 1) was obtained with a spatial resolution of 1.0° x 1.0° from the Global Precipitation Climate Centre (GPCP, <https://www.dwd.de/EN/ourservices/gpcc/gpcc.html>), and then converted into monthly data (mm month<sup>-1</sup>).

## 2.6. Wavelets

Time series of oceanographic parameters are composed of several oscillatory signals, which can be decomposed through spectral analysis. In

order to evaluate the spatio-temporal variability of SSC time series, the wavelet analysis was used in this study. The wavelet analysis is a common and powerful tool for detecting signals and localizing variations of power within time series (Doglioni and Simione, 2014). This analysis provides frequency-time space information, which enables to determine dominant modes of variability and how those modes vary in time (Torrence & Compo, 1998).

For the present study, a discrete analysis (1-D wavelet) was applied to precipitation and SOI timeseries based on Daubechies (1992) using a long-term process decomposition filter. Yet, as the Morlet and Mexican hat mother-wavelets are the most used wavelets to analyse hydrological variables (Marques *et al.*, 2014; Oliveira *et al.*, 2015; Costi *et al.*, 2018), they were used in the present study to analyse wind intensity and river discharge relations with SSC, respectively.

### 3. Results and Discussion

#### 3.1. SSC Variability

Figure 4 presents the temporal evolution of calculated SSC for the 5-years simulation and river discharge data measured at Guaíba River, Camaquã River and São Gonçalo Channel (Figures 4a, 4b, 4c) for the same period. Results indicated that during this 5-years period the Guaíba River, Camaquã River and São Gonçalo Channel had mean discharges of  $1326.5 \text{ m}^3\cdot\text{s}^{-1}$ ,  $365.6 \text{ m}^3\cdot\text{s}^{-1}$ ,  $871.4 \text{ m}^3\cdot\text{s}^{-1}$ , respectively. The overall continental contribution had a mean discharge of  $2563.5 \text{ m}^3\cdot\text{s}^{-1}$ , higher than the historical mean (Vaz *et al.*, 2004). Calculated SSC time series for this period showed a direct correlation with river discharge (Guaíba river,  $r=0.84$ ; Camaquã River,  $r=0.73$ ; São Gonçalo Channel,  $r=0.77$ ), where an increase (decrease) in river discharges results in an increase (decrease) in SSC, with differences related to the Patos Lagoon residence time (Fernandes *et al.*, 2002).

The calculated SSC time series shows a clear pattern, with higher values at wet periods, (max SSC  $180 \text{ mg}\cdot\text{L}^{-1}$ ), and lower values during dry periods (max SSC  $20 \text{ mg}\cdot\text{L}^{-1}$ ). The highest SSC were observed in 2002, when the Guaíba river discharge reaches  $10,020 \text{ m}^3\cdot\text{s}^{-1}$  and the São Gonçalo Channel

2,500 m<sup>3</sup>.s<sup>-1</sup>, and in 2005 when the Guaíba river outflow was about 10,786 m<sup>3</sup>.s<sup>-1</sup>. Apart from the well-known river discharge and SSC relation, winds seem to be also important. At the Patos Lagoon, winds (Figure 4d) follow a NE-SW regime (Moller *et al.*, 2001; Castelão and Möller, 2003). For the whole period, NE winds were dominant, and ranged from -1.7 m.s<sup>-1</sup> to -7.5 m.s<sup>-1</sup>. Yet, this wind regime promotes SSC transport along the lagoon towards the coast. Although SW winds are less often, they are more intense, with greater wind speeds ranging from 1.35 m.s<sup>-1</sup> to 11.8 m.s<sup>-1</sup>, and promote flood fluxes at the estuarine area (Moller *et al.*, 2001; Castelão and Möller, 2003), and water accumulation within the lagoon.

In addition, monthly means were calculated based on 2002-2006 daily time series of SSC at Guaíba and Camaquã rivers, and São Gonçalo Channel (Figure 4e, 4f, 4g). Overall, SSC increases from January to June, mainly at Guaíba river mouth, and a decrease in July. At São Gonçalo (Figure 4f), SSC decrease from July to December. In contrast, at Guaíba (Figure 4d) and Camaquã (Figure 4e) rivers, SSC increases from August to October and decreases from November to December.

At Guaíba river (Figure 4e), SSC is about 13 mg.L<sup>-1</sup> during summer, increasing its concentration during fall. During winter, SSC is about 50 mg.L<sup>-1</sup> and its maximum is observed during spring, with 75 mg.L<sup>-1</sup>. The Camaquã river (Figure 4f), on the other hand, showed a distinct pattern: 15 mg.L<sup>-1</sup> during summer, with an increase to approximately 40 mg.L<sup>-1</sup> during fall, winter and spring, and with lower SSC in July (29 mg.L<sup>-1</sup>). The same pattern is observed at São Gonçalo channel (Figure 4g): lower SSC during summer, where SSC is about 23 mg.L<sup>-1</sup>, reaching its maximum during fall (50 mg.L<sup>-1</sup>), followed by a decrease during winter (34 mg.L<sup>-1</sup>) and spring (37 mg.L<sup>-1</sup>). Also, note that the SSC fluctuations at Camaquã river present a smaller amplitude than the ones observed at Guaíba river and São Gonçalo Channel (Figure 4d, 4e, 4f).

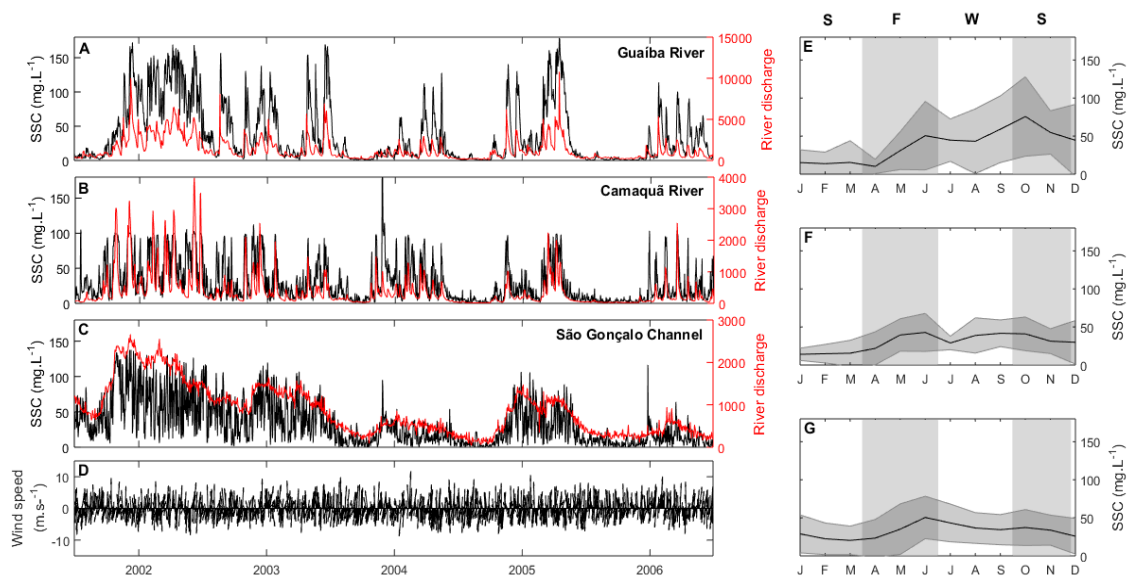


Figure 4 – Temporal evolution of calculated SSC and river discharge for the 5-years period at a) Guaíba River, b) Camaquã River, and c) São Gonçalo Channel. Wind speed is shown in d, where negative (positive) values represent NE (SW) winds. Monthly mean timeseries (2002-2006) of SSC (black,  $\text{mg.L}^{-1}$ ) at e) Guaíba River, f) Camaquã River, and g) São Gonçalo Channel. Standard deviations are shown in grey shading for SSC.

Figure 5 presents the calculated five years SSC austral seasonal means. During winter (Figure 5c), high SSC ( $\approx 50 \text{ mg.L}^{-1}$ ) are observed near the tributaries mouth, while in the centre of the lagoon, SSC remain low ( $\approx 5 \text{ mg.L}^{-1}$ ). The same pattern is observed over spring (Figure 5d), in which SSC is intensified and spread throughout the lagoon. During summer (Figure 5a), SSC are reduced ( $\approx 20 \text{ mg.L}^{-1}$ ) at the north and mid-lagoon, however, they are still higher than SSC over fall (Figure 5b), which can reach  $\approx 5 \text{ mg.L}^{-1}$ . Pasquini *et al.* (2012) observed the same pattern when analysing river discharge on Patos Lagoon: higher values over winter and early spring, and low to intermediate during summer and fall.

At the estuarine area (Figure 5e, 5f, 5g, 5h), SSC is higher near São Gonçalo Channel mouth, decreasing its concentration towards the coastal zone. Mainly, there is an increase in SSC during winter (Figure 5g) and spring (Figure 5h) related to an increase in São Gonçalo outflow and the predominance of NE winds, which favours ebb events, and tend to transport SSC over larger distances, reaching the coastal zone. During summer (Figure 5e) and fall (Figure 5f), on the other hand, with weak NE regime, SSC seems to be lower,

decreasing its intensity throughout the estuary. Even though the Patos Lagoon SSC showed large spatial and temporal variability among the tributaries (Figure 4) throughout the years, they indicate a general trend of lower concentrations in summer-fall than in winter-spring.

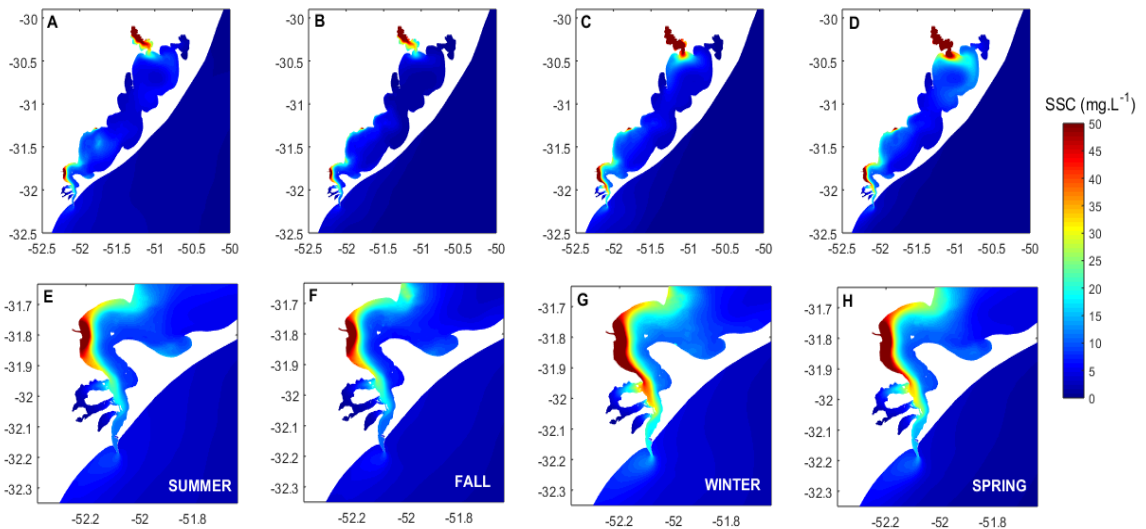


Figure 5 – Five years (2002-2006) calculated SSC means for the austral seasons: a) summer (DJF), b) fall (MAM), c) winter (JJA), and d) spring (SON). Zoom for the estuarine area are shown for e) summer, f) fall, g) winter, and h) spring.

In coastal environments that receive significant contributions from river discharges, the wind plays a secondary role on the SSC dynamics (Mendes *et al.*, 2017), but modulates its shape and orientation (Geyer *et al.*, 2004). At the Patos Lagoon, wind forcing seems to present a secondary role on SSC behaviour, together with river discharges. Aside from river discharge effects, Figure 6 presents snapshots of the Patos Lagoon's SSC response during specific wind directions (N, NE, E, SE, S, SW, W, NW). N, NE, and NW regimes (Figure 6) induce an SSC southward movement. NE (NW) winds promote Guaíba and Patos Lagoon coastal plumes expansion to the east (west). However, during S, SE and SW regimes, the SSC pattern is the opposite: there are SSC fluxes towards the inner lagoon, confining SSC into the water body. SE and SW winds promote the SSC transport to mid and north-lagoon and reallocate SSC to isolated portions. Finally, E and W winds tend to push SSC to east and west lagoon's portions, respectively, potentially eroding its margins.

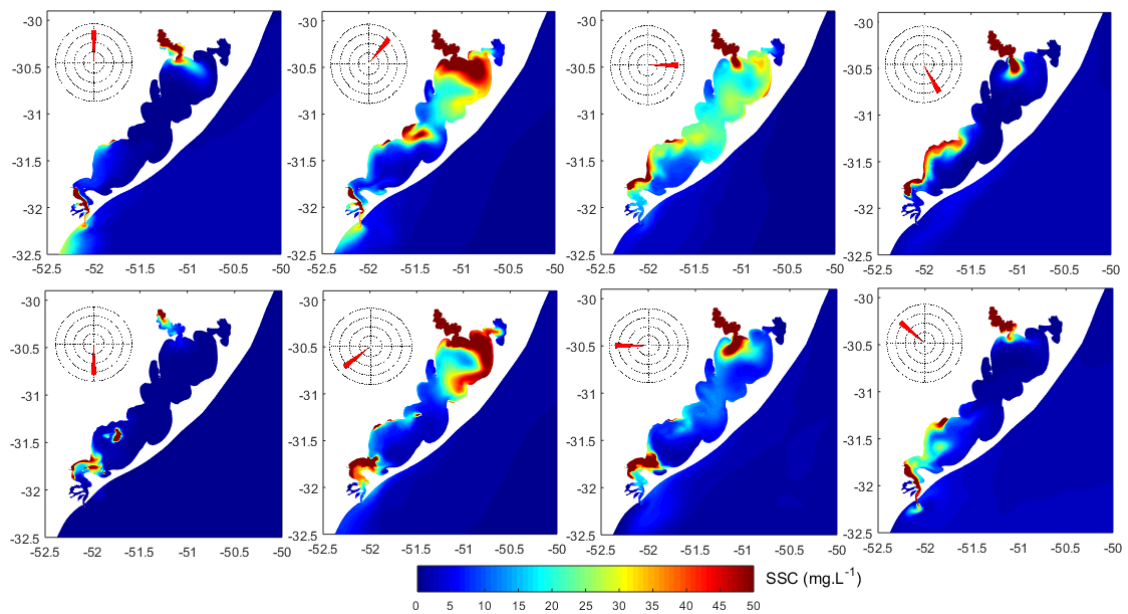


Figure 6 – Influence of winds on SSC behaviour.

The spatio-temporal variability of SSC in the Patos Lagoon was characterized by daily SSC time series extracted from the modelling results at selected sites (Figure 1) for the period between 2002-2006 (Figure 7a). Daily anomalies for river discharge and wind speed, monthly precipitation rates and SOI index are presented in Figures 7b, 7c, 7d, and 7e, respectively. At the north of the lagoon (Figure 7a), the well-defined SSC contributions from Guaíba River can be observed in most of the years, where SSC are high and can be dispersed for several kilometres under NE wind regime.

On the other hand, at mid-lagoon, SSC are low (Figure 7a), once Camaquã SSC supplies are restricted to a small area, being its contribution more significant in the estuarine zone, mainly during NE wind influence. At the estuarine portion, SSC pattern is more variable, once this area is strongly affected by São Gonçalo Channel and Camaquã outflow, by the wind (NE-SW) influence, and it has a restricted influence of the tides (Fernandes *et al.*, 2004; Marques *et al.*, 2010). During NE winds (Figure 7c, negative values) and higher river discharges, SSC enhance the formation of plumes at the coastal zone, which can be transported throughout 18 days (Pereira and Niencheski, 2004). During SW winds (Figure 7c, positive values) and lower river discharges, on the other hand, the SSC flows towards the mid-lagoon. Yet, due to salinity intrusions, SSC seems to show a distinct pattern, which can be associated to



flocculation and sediment deposition processes (Van Leussen, 1999). According to Pereira and Niencheski (2004), under these conditions, it takes about 38 days to SSC be transported throughout the lagoon.

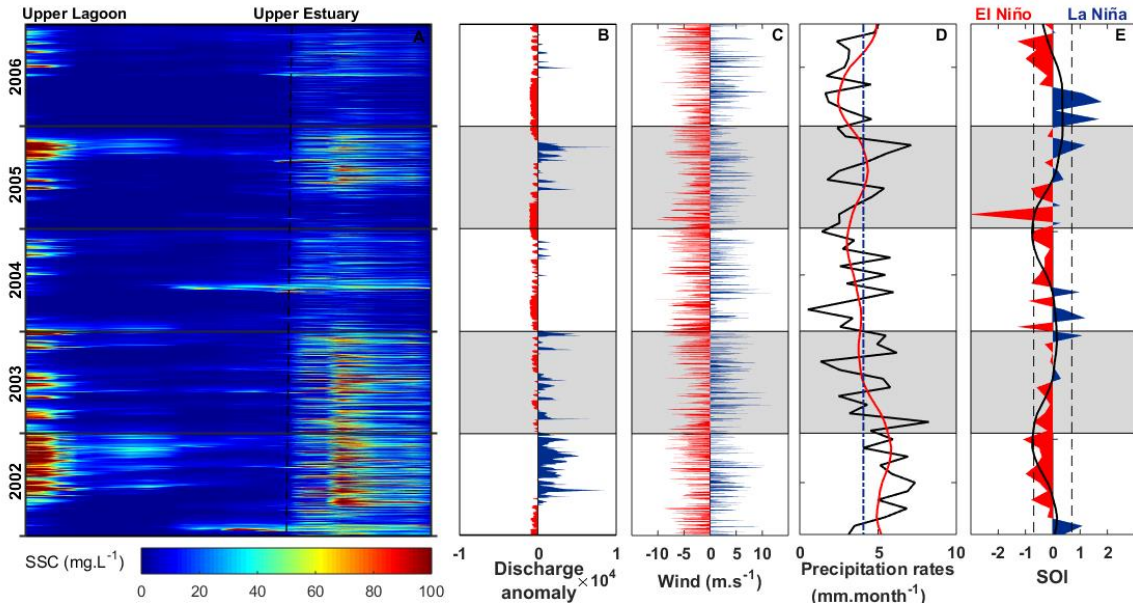


Figure 7 – a) Spatio-temporal distribution of SSC (mg.L<sup>-1</sup>) along the Patos Lagoon (see Figure 1 for location). b) Guaíba River discharge anomaly (m<sup>3</sup>.s<sup>-1</sup>). Positive (negative) Guaíba river outflow anomaly is shown in blue (red). c) wind speed, where negative (positive) values represent NE (SW) winds; d) precipitation rates (black), its mean (blue) and long-term trend (red); and e) SOI and its long-term trend (black). Dashed lines between -0.7 and 0.7 represent periods of neutral years.

Moreover, the interannual variability of SSC throughout the years is clearly observed and seems to be related to river discharges, winds, precipitation rates, and ENSO events (Figures 7b, 7c, 7d, 7e). NE winds, high precipitation rates, river discharges and SSC values along the lagoon in mid-2002-2003 occur during El Niño events. During La Niña events (2004 and 2006), with higher incidence of SW winds, lower precipitation rates and river discharge, SSC values appear to be low (Figure 7a). As an exception, the high SSC, precipitation rate, and river discharge anomaly observed in 2005 is not associated with an El Niño event. This particular year can be possibly associated with a neutral year.

ENSO-triggered events are well recognized in South America, particularly on precipitation rates (Grimm and Tedeschi, 2009; Pasquini *et al.*, 2012), directly affecting river discharges (Möller *et al.*, 2009). At the Patos Lagoon, it produces an increase (decrease) in precipitation rates (Figure 7d, red

line) and river discharges (Figure 7b) at interannual timescales, resulting in an increase (decrease) in SSC, that can be attributed to El Niño (La Niña) events (Figure 7e). An exception for this behaviour is observed in 2004-2005. The same river discharge pattern was observed by Pasquini *et al.* (2012) when analysing SOI, precipitation rates and river discharge in the south of Brazil: higher (lower) values during El Niño (La Niña) years. Although river discharges can be a reasonable explanation for the seasonal and interannual SSC patterns found in the present study, it must not be the only factor.

Another important factor can be the strength of ENSO events, which directly affects the intensity of river discharges and wind regimes patterns. Aside from river discharges effects, Möller *et al.* (2009) and Marques *et al.* (2010) observed the Patos Lagoon wind patterns over ENSO events. Over El Niño years, NE winds are dominant and intensified. This pattern promotes ebb events and decreases suspended sediments deposition. During neutral years, NE winds are also dominant, but SW winds are better distributed. In contrast, over La Niña years SW winds are more frequent and stronger, resulting from the passage of successive meteorological cold fronts (Möller *et al.*, 2009). The latter wind regime promotes water accumulation within the lagoon.

Opposed to what is observed by Dogliotti *et al.* (2016) at Río de La Plata, in which not all rivers are influenced by ENSO events, at the Patos Lagoon all the major rivers seem to be affected by ENSO events, which affect SSC patterns (Figure 7a, 7b). In turn, higher amplitudes in SSC seasonal cycle can be observed in years when the Patos Lagoon outflow is higher than average and is more pronounced in years associated with El Niño events, and the opposite pattern is observed in La Niña events.

### 3.2. *The estuarine behaviour*

The water level differences at the estuarine zone (Figure 1, points 2 and 8) is shown in Figure 8a. The difference was calculated by subtracting water level values of point 2 from point 8. Also, wind speed and calculated SSC data for the selected points are presented in Figure 8b, 8c. For wind speed, it was only considered NE/SW winds, once they are predominant at the study area.

Positive (negative) water level difference values (Figure 8a) indicate ebb (flood) periods. Barros *et al.* (2012) state that river discharge influence on water level differences at estuarine area is about 50%. Aside from river discharges influence, winds seem to play an important role in water level fluctuations. The relation between water level difference and winds is noticeable (Figure 8a, 8b), with an inverse correlation ( $r=-0.64$ ), confirming that increases (decreases) in water level difference values are directly related to NE (SW) winds predominance.

Besides, positive (negative) water level differences promote depression (elevation) in coastal sea surface, generating the barotropic pressure gradient, and resulting in seaward (landward) flows between the lagoon and the coast. Fernandes *et al.* (2002) explain that the strength of the pressure gradient is intimately connected with the strength of winds and river discharges, also affecting water advection into or out of the lagoon. Moreover, positive (negative) water level differences are related to high (low) SSC (Figure 8c), which is possibly related to SSC transport. Mainly, during 2002 and 2003, it is observed an increase in water level difference, predominance of NE winds, and an increase in SSC. It may happen as a result of El Niño events over these years, which turns ebb events favourable. In turn, during 2004 and 2006, water values differences are lower or negative and SSC are lower as a result of a dry season caused by La Niña events.

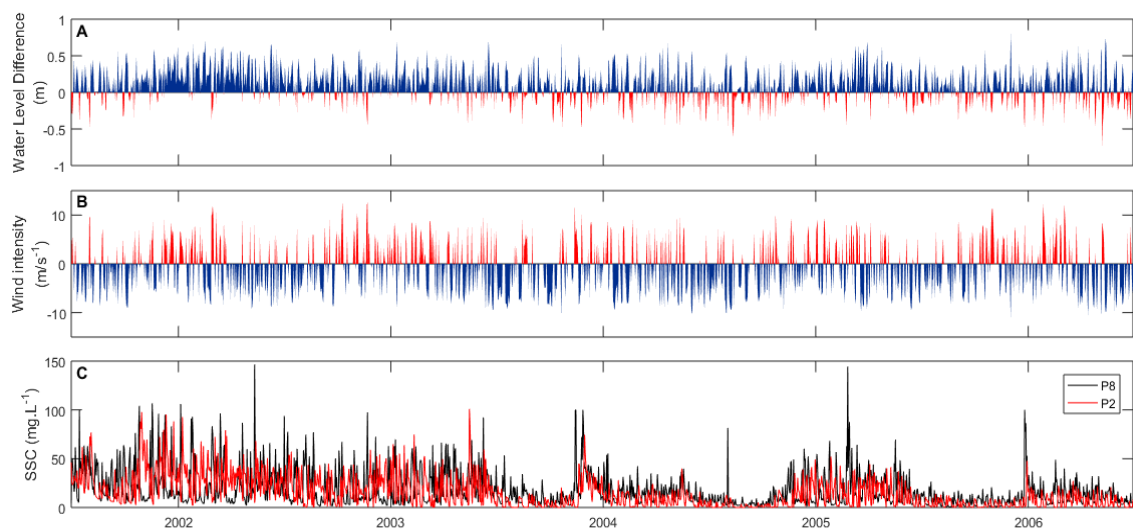


Figure 8 – a) Water level differences between points 8 and 2 (see Figure 1 for location). Ebb (Flood) events are presented in blue (red). b) Wind speed. Negative

(Positive) values shown in blue (red) represent NE (SW) winds; c) calculated SSC data for points 2 and 8.

The relation between calculated SSC and salinity is illustrated by time series extracted from points 8, 6, 4, and 2 (Figure 1) for 2002-2006 (Figure 9). Results reflect the salinity and SSC pattern: an increase (decrease) in salinity coincides with a decrease (increase) in SSC. Pearson correlation coefficient between salinity and SSC time series (Table 3) showed an inverse correlation between the selected points, being more significant at points 6 and 2.

Table 3 – Statistical analysis between SSC and Salinity.

Station	Pearson Correlation	<i>p</i> -value
P8	-0.1478	< 0.00001
P6	-0.6208	< 0.00001
P4	-0.5338	< 0.00001
P2	-0.6029	< 0.00001

Point 8 (Figure 9a) is located at the estuary boundary and near the river discharge source (Camaquã river and São Gonçalo Channel), which promotes subtler SSC x Salinity changes. A similar pattern is observed at point 6 (Figure 9b), however, with higher SSC due to the direct influence of São Gonçalo Channel outflow. Points 4 (Figure 9c) and 2 (Figure 9d) show a similar behaviour, with higher concentrations on point 4, and a more intense influence of salinity on both points. Nevertheless, in general, decreases in SSC are possibly caused by deposition and flocculation of SSC. Laboratory experiments indicated an enhance in the settling and flocculation process on saline waters due to cohesive sediments characteristics (Chandra *et al.*, 2010; Portela *et al.*, 2013). Van Leussen (1999) demonstrated, based on field measurements in Ems estuary and complementary laboratory experiments, the effect of salinity in the settling velocity of SSC, and he observed that in high-salinity regions, there is a significant increase in the settling velocity and flocculation of SSC.

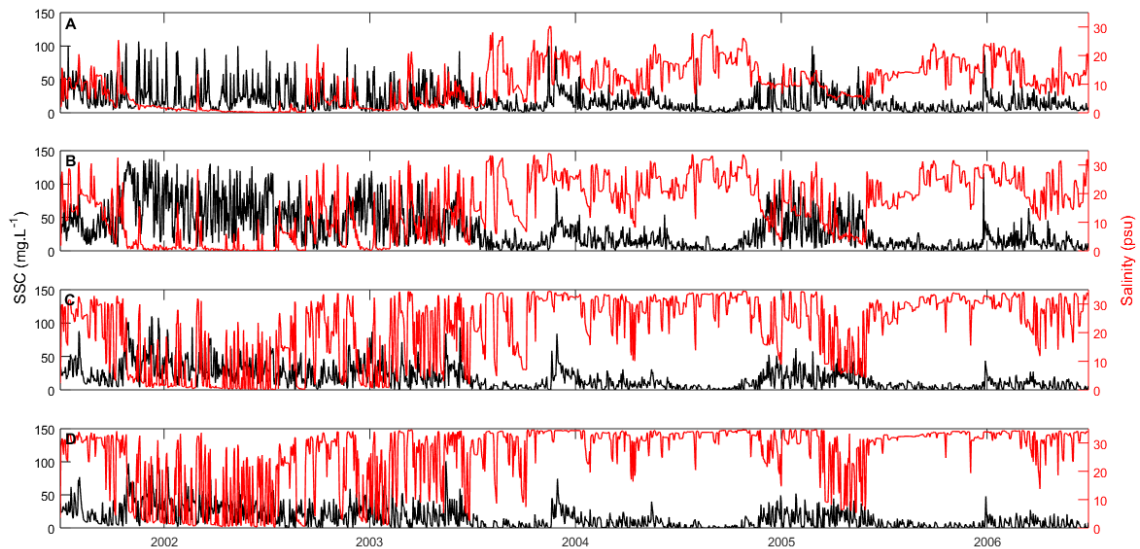


Figure 9 – Spatial and temporal variations of calculated SSC and salinities at points (a) 8, (b) 6, (c) 4, and (d) 2 for the simulated period (2002-2006).

### 3.3. SSC Spatio-Temporal Variability

Calculated time series of SSC and river discharge and wind data at P2, P8 and P24 (Figure 1), the cross-wavelet analysis and the global power spectrum between the time series are shown in Figures 10, 11 and 12, respectively. Results indicated that at the estuarine mouth (P2, Figure 1), the relation between the discharge and the calculated SSC (Figure 10a) occurs mainly in a time interval between 128 and 256 days in 2002 - 2003, changing to 128 - 512 days in 2004 – 2005 (Figure 10b), suggesting a seasonal influence together with an interannual signal, also indicating ENSO influence on both variables. The correlation between both time series occurring only in a time interval bigger than 128 days is also evident in the global spectrum (Figure 10c). The relation between the wind and SSC (Figure 10d) time series at the mouth of the estuary (P2, Figure 1), on the other hand, occurs in a time interval between 2 and 16 days (Figure 10e and 10f), indicating the influence of synoptic winds on the SSC dynamics at this area.

At upper estuary (P8, Figure 1), results indicated the relation between the discharge and the calculated SSC (Figure 11a) occurring mainly in a time interval between 256 and 512 days in 2002 - 2003 and 2004 – 2005 (Figure 11b), suggesting a seasonal influence together with an interannual signal, i.e., ENSO influence. The correlation between both time series occurring only in a

time interval bigger than 256 days is also evident in the global spectrum (Figure 11c). Nonetheless, the relation between the wind and SSC (Figure 11d) time series at upper estuary (P8, Figure 1) occurs in a time interval between 2 and 16 days (Figure 11e and 11f), indicating the influence of synoptic winds on the SSC dynamics at this area.

When moving to the north of the lagoon (P24, Figure 1), the relation between the discharge and the calculated SSC (Figure 12a) occurs in intervals between 64 and 512 days in 2002-2003 and 2005, changing to 512 in 2004 (Figure 12b), suggesting a seasonal and interannual influence (ENSO influence). The global power spectrum (Figure 12c) corroborates with these results, showing that the correlation between both timeseries is bigger than 64 days. On the other hand, results did not indicate a relation between wind and SSC (Figure 12d) timeseries at the north of the lagoon (P24, Figure 1). The global power spectrum (Figure 12e) indicates no influence of wind action at P24, probably due to the strong and dominant influence of river discharge at this location.

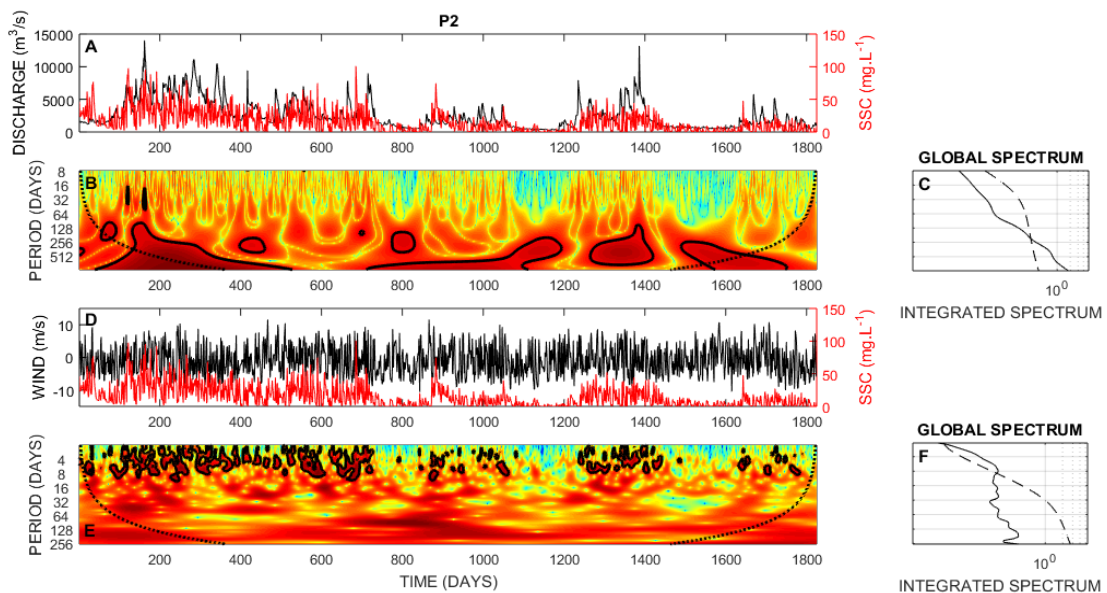


Figure 10 – At P2: a) Time series of the river discharge (black) and SSC (red). (b) Local energy cross-spectrum using the Mexican hat wavelet. The contour lines enclose regions with 95% confidence interval. The dashed line indicates the cone of influence where the edge effects become important. (c) The time-averaged wavelet power spectra. The dashed line represents the 95% confidence level. (d) Time series of wind intensity (black) and SSC (red). (e) Local energy cross-spectrum using the Morlet wavelet. The contour lines enclose regions with 95% confidence interval. The dashed

line indicates the cone of influence where the edge effects become important. (f) The time-averaged wavelet power spectra. The dashed line represents the 95% confidence level.

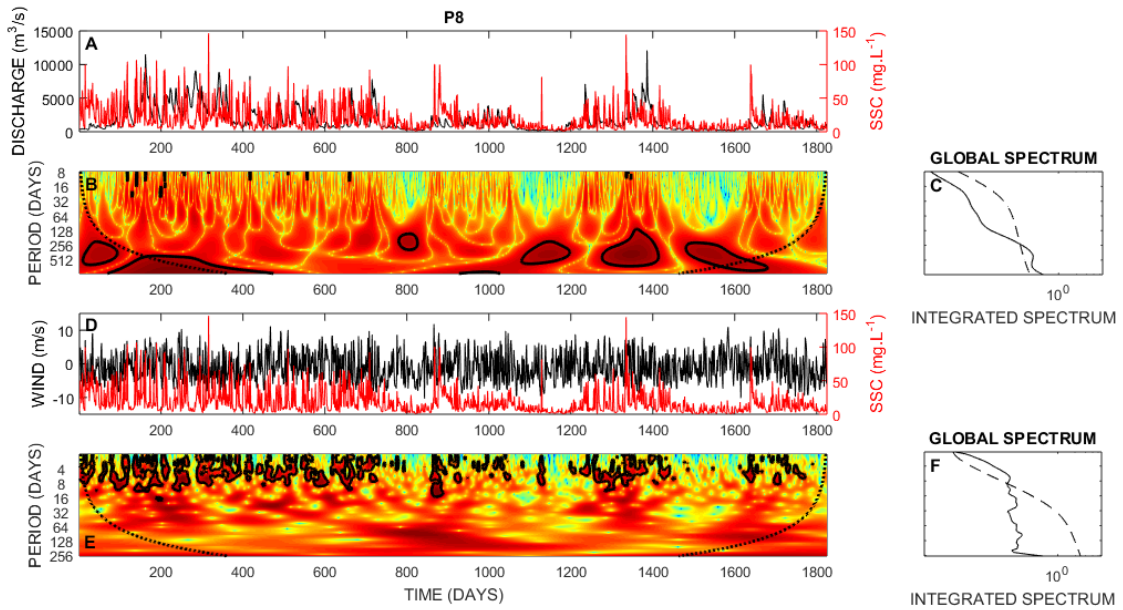


Figure 11 – At P8: A) Time series of the river discharge (black) and SSC (red). (b) Local energy cross-spectrum using the Mexican hat wavelet. The contour lines enclose regions with 95% confidence interval. The dashed line indicates the cone of influence where the edge effects become important. (c) The time-averaged wavelet power spectra. The dashed line represents the 95% confidence level. (d) Time series of wind intensity (black) and SSC (red). (e) Local energy cross-spectrum using the Morlet wavelet. The contour lines enclose regions with 95% confidence interval. The dashed line indicates the cone of influence where the edge effects become important. (f) The time-averaged wavelet power spectra. The dashed line represents the 95% confidence level.

Overall, the wavelet analysis suggests that the Patos Lagoon is dominated by winds on shorter timescales and by river discharges on longer timescales. The global spectrum agrees with these statements, showing values below the mean at shorter (wind influence) and longer (river discharges influence) time scales. Yet, results also show the interannual influence of ENSO events on both analyses, as seen in 2002 and 2004 (Figure 10b, 11b, and 12b), for example. Marques (2012) points out the high interannual variability of river discharges on Patos Lagoon, which can intensify (reduce) the seasonal discharge pattern during El Niño (La Niña) years. Barros and Marques (2012), when analysing river discharges influence on the Patos Lagoon, observed a similar pattern.

In shorter time scales, there is the predominance of wind alternation processes, directly related to front passages (Moller *et al.*, 2001). In addition, the presence of mobile cyclones and anticyclones in the South Atlantic Ocean contributes to wind variability at Patos Lagoon. Moller *et al.* (2001), Castelão and Moller (2003), and Fernandes *et al.* (2004, 2005) also observed the influence of winds on the Patos Lagoon circulation during periods from 3 to 16 days. Costi *et al.* (2018), when studying Mirim-São Gonçalo System, observed similar patterns for both correlations. Meccia *et al.* (2013) concluded that the NE-SW winds alternation modulate the intra-seasonal SSC patterns variability, becoming the major forcing on short timescales variability, which is in agreement with the results from this study.

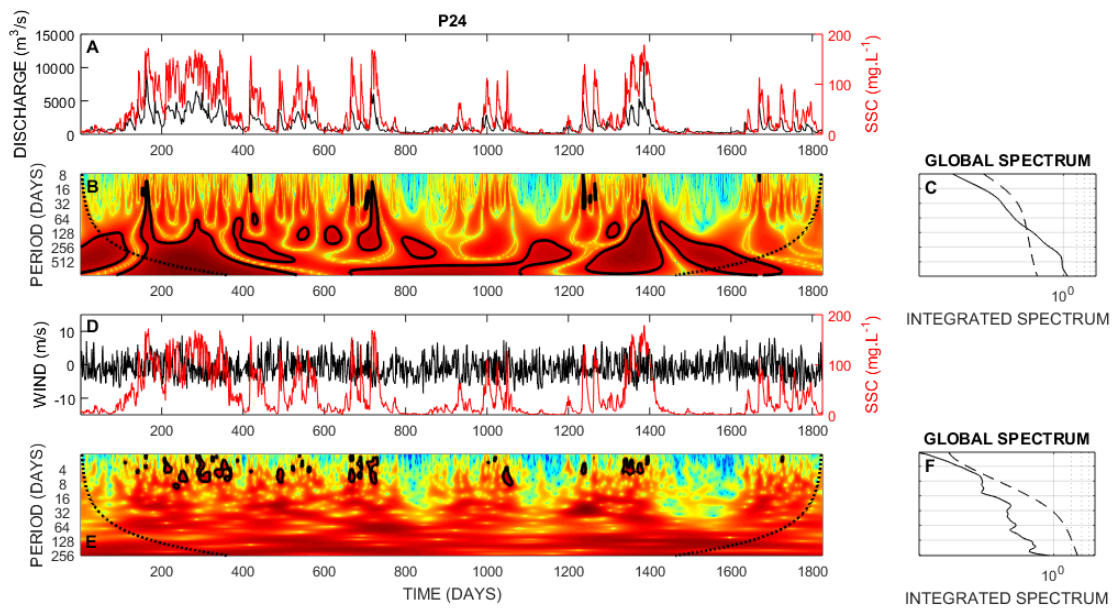


Figure 12 – At P24: A) Time series of the river discharge (black) and SSC (red). (b) Local energy cross-spectrum using the Mexican hat wavelet. The contour lines enclose regions with 95% confidence interval. The dashed line indicates the cone of influence where the edge effects become important. (c) The time-averaged wavelet power spectra. The dashed line represents the 95% confidence level. (d) Time series of wind intensity (black) and SSC (red). (e) Local energy cross-spectrum using the Morlet wavelet. The contour lines enclose regions with 95% confidence interval. The dashed line indicates the cone of influence where the edge effects become important. (f) The time-averaged wavelet power spectra. The dashed line represents the 95% confidence level.

### 3.4. Future Studies



Future efforts focusing on the waves influence on SSC in the Patos Lagoon would increase our understanding of SSC dynamics and sediment transport processes. In addition, the combination of in-situ measurements, morphodynamical modelling and remote sensing techniques would enhance our knowledge about SSC structure, values, and other sources, such as discards from crops fields and navigation activities throughout the Patos Lagoon and its estuarine area.

#### 4. Conclusions

The present study provides detailed information about SSC dynamics in the Patos Lagoon throughout a five-years period. Although it is a medium-term simulation, it shows the usefulness of using numerical models as a suitable tool for monitoring SSC on coastal environments. Based on calculated SSC data, our results showed the strong relation between SSC and river discharges (from Guaíba river, Camaquã river, and São Gonçalo channel), indicating river discharge influence over SSC. Mainly, SSC from Guaíba river, Camaquã river, and São Gonçalo channel show a clear pattern: higher values at wet periods and lower values during dry periods. Moreover, the study showed the SSC seasonal pattern: higher values during winter and spring, and low to moderate during summer and fall. Also, the wind influence was observed on SSC propagation over the lagoon, with SSC transport mainly controlled by NE (SW) winds towards the estuary (inner lagoon). Afterwards, SSC analysis from Guaíba river showed a well-defined pattern and being dispersed for several kilometres. SSC from Camaquã river together with São Gonçalo channel, on the other hand, provided significant contributions only for the estuarine zone, where they are subjected to salinity influences on SSC. Meanwhile, ENSO illustrated its influence on interannual variability, rising SSC amplitudes during El Niño years and decreasing SSC during La Niña years by affecting atmospheric conditions, reflecting on precipitation rates, wind actions and river discharges. At the estuarine area, the SSC seems to be directly related to water level difference and inversely related to salinity, which directly affects sedimentation processes. Overall, SSC on Patos Lagoon is dominated by river

discharges from seasonal to interannual timescales, being intensified on point 24, and by winds at synoptic timescales, especially on points 2 and 8. No correlation was found between SSC and wind intensity on point 24, indicating no wind influences on SSC.

### **Acknowledgements**

The authors are grateful to the Brazilian Improving Coordination of Higher Education Personnel (CAPES) and the Federal University of Rio Grande (FURG) for financial support. The authors are also thankful to Dr. Osmar Möller, from Institute of Oceanography at FURG, for supplying salinity and current velocities data; to the Dr. Carlos Augusto Schettini, from Oceanography Department at Federal University of Pernambuco, for SSC data. The Telemac model is an open source model available at <http://www.opentelemac.org/>. The temperature and salinity data from HYCOM + NCODA Global (*HYbrid Coordinate Ocean Model*) Project are available at <https://hycom.org/>. ERA-Interim wind data from ECMWF is available at <http://www.ecmwf.int/>. The river discharge and water level data can be obtained, respectively, from Brazilian National Water Agency (ANA, [www.hidroweb.ana.gov.br](http://www.hidroweb.ana.gov.br)) and Mirim Lagoon Agency (ALM, <https://wp.ufpel.edu.br/alm/>). Monthly Southern Oscillation Index (SOI) data can be obtained from <https://www.esrl.noaa.gov/psd/enso/soi>. Daily precipitation data can be obtained at <https://www.dwd.de/EN/ourservices/gpcc/gpcc.html>.

# **Capítulo V:**

## Considerações Finais

## 5. Considerações Finais

O presente estudo analisou a variabilidade espaço-temporal das concentrações de sedimento em suspensão na Lagoa dos Patos através de cinco anos de simulações hidrodinâmicas + CSS pelo modelo TELEMAC – 3D. Os resultados mostraram alta correlação ( $r \approx 0,8$ ) entre as CSS e a descarga dos rios, principalmente do Rio Guaíba. Além disso, um padrão (Figura 4, manuscrito) foi observado nos três tributários: altas (baixas) CSS nos períodos úmidos (secos). Ademais, a CSS mostrou um padrão sazonal (Figura 5, manuscrito) similar ao das descargas dos rios, onde se observou altas concentrações durante o inverno e primavera, e moderada a baixas concentrações durante o verão e outono.

O papel do regime NE-SO de vento foi observado na propagação das CSS ao longo da lagoa, onde durante o regime NE (SO), o transporte das CSS é em direção a (ao) região estuarina (interior da lagoa), padrão esse já observado por Möller *et al.* (2001) e Castelão e Möller (2003) ao analisarem a hidrodinâmica da lagoa. As CSS (Figura 7, manuscrito) provenientes do Rio Guaíba mostraram um padrão bem definido e a dispersão dessas CSS ao longo da lagoa. Em contrapartida, as contribuições das CSS provenientes do Rio Camaquã e Canal São Gonçalo (Figura 7, manuscrito) abrangeram somente a região estuarina, a qual está sujeita aos efeitos da floculação devido a presença do sal. Já na escala interanual, a influência dos eventos ENSO foi observada. Durante anos de El Niño (La Niña), as CSS foram aumentadas (reduzidas) devido aos seus efeitos nas condições atmosféricas, refletindo nas taxas de precipitação, ação dos ventos e descargas dos rios.

Na porção estuarina, uma comparação mostrou a relação direta entre as CSS e desnível (Figura 8), o qual está intimamente relacionado com a ação dos ventos. Além disso, foi observado uma relação inversa com a salinidade (Figura 9), provavelmente devido aos efeitos da floculação no sedimento em contato com a água salgada, afetando, assim, os processos de sedimentação. De forma geral, as CSS nesse ambiente mostraram-se dominadas pela ação das descargas dos rios em escalas sazonais a interanuais e pelos ventos em

escalas sinópticas, exceto no ponto 22 (Figura 12, manuscrito), onde não foi observada correlação entre o vento e as CSS.

Trabalhos futuros focando em analisar a influência das ondas nas CSS na Lagoa dos Patos devem melhorar nosso entendimento referente a dinâmica das CSS e os processos sedimentares. Ademais, a combinação de dados em situ, modelagem morfodinâmica e sensoriamento remoto ampliariam nosso conhecimento em termos de distribuição horizontal e vertical, além de uma análise quantitativa e, também, considerar outras fontes de sedimentos, tais como provenientes das lavouras e de dragagem, o que não foi possível no presente trabalho. Outra sugestão, que não pôde ser feita nesse trabalho, seria identificar as principais zonas de erosão do sedimento de fundo e de deposição do sedimento em suspensão ao longo da Lagoa dos Patos através de um modelo morfodinâmico.

## Referências Bibliográficas

- Andrade Neto, J.; Rigon, L.; Toldo Jr, E.; Schettini, C. (2012). Descarga sólida em suspensão do sistema fluvial do Guaíba, RS, e sua variabilidade temporal. *Pesq. em Geociências*, 39(2): 161-171.
- Barros, G.P.; Marques, W.C. (2012). Long-term temporal variability of the freshwater discharge and water levels at Patos Lagoon, Rio Grande do Sul, Brazil, *International Journal of Geophysics*. doi:10.1155/2012/459497.
- Bedri, Z., Bruen, M., Dowley, A., Masterson, B. (2013). Environmental consequences of a power plant shut-down: A three-dimensional water quality model of Dublin Bay. *Marine Pollution Bulletin*, 71, 117-128.
- Callari, L.J. (1980). Aspectos sedimentológicos e ambientais da região sul da Lagoa dos Patos. Universidade Federal do Rio Grande do Sul, Instituto de Geociências. 190p. (Dissertação de Mestrado).
- Calliari, L.J., Winterwerp, J.C., Fernandes, E., Cuchiara, D., Vinzon, S.B., Sperle, M. & Holland, K.T. (2009). Fine grain sediment transport and deposition in the Patos Lagoon–Cassino beach sedimentary system. *Continental Shelf Research*. 23: 515-529. Doi:10.1016/j.csr.2008.09.019
- Castelão, R. M. and Moller Jr, O. O. (2003). 'Sobre a circulação tridimensional forçada por ventos na lagoa dos patos', *Revista Atlantica*, 25(2001), pp. 91–106.
- Chandra, V.; Mohapatra, P. L.; Hillebrand, G.; Nestmann, F. (2010). Effect of Salinity on Suspended Cohesive Sediments. *International Review of Civil Engineering*.
- Costi, J., Marques, W. C., Kirinus, E. P., Duarte, R. F., Arigony-Neto, Jorge. (2018). Water level variability of the Mirim - São Gonçalo system, a large, subtropical, semi-enclosed coastal complex. *Advances in Water Resources*, p. 75-86.
- Daubechies, I. (1992). *Ten Lectures on Wavelets*, CBMS-NSF Regional Conference Series in Applied Mathematics. Philadelphia, PA: SIAM Ed.
- Dogliani, A. and Simeone, V. (2014). Geomorphometric analysis based on discrete wavelet transform, *Environmental Earth Sciences*, 71(7), pp. 3095–3108. doi: 10.1007/s12665-013-2686-3.
- Dogliotti, A. I., Ruddick, K. and Guerrero, R. (2016). Seasonal and inter-annual turbidity variability in the Río de la Plata from 15 years of MODIS: El Niño dilution effect, *Estuarine, Coastal and Shelf Science*. Elsevier Ltd, 182, pp. 27–39. doi: 10.1016/j.ecss.2016.09.013.
- Egbert, G.; Erofeeva, S. (2002) Efficient inverse modeling of barotropic ocean tides. *Journal of Atmospheric and Oceanic Technology* 19:183-204.
- Etemad-Shahidi, A., Shahkolahi, A., Liu, W.-C. (2010). Modeling of hydrodynamics and cohesive sediment processes in an estuarine system: study case in Danshui River. *Environ. Model. Assess.*, 15 (4), pp. 261-271.
- Fassoni-Andrade, A.; Guasselli, L.; Toniolo, G.; Moreira, A. (2015). Dinâmica espacial e temporal de sedimentos em suspensão na região estuarina da Lagoa dos Patos - RS, a partir de dados do sensor OLI, Landsat-8, 7, 6381-6388.

Fernandes, E.; Dyer, K.; Möller, O.; Niencheski, L. (2002) The Patos Lagoon hydrodynamics during an El Niño event (1998), *Continental Shelf Research*, 22(11–13), 1699–1713. doi: 10.1016/S0278-4343(02)00033-X.

Fernandes, E.; Mariño-Tapia, I.; Dyer, K.; Moller, O. (2004) The attenuation of tidal and subtidal oscillations in the Patos Lagoon estuary, *Ocean Dynamics*, 54(3–4), pp. 348–359. doi: 10.1007/s10236-004-0090-y.

Fossati, M; Piedra-Cueva, I. (2008). Numerical modelling of residual flow and salinity in the Río de la Plata. *Applied Mathematical Modelling*, 32, 1066-1086.

Garcia, A.M., Vieira, J.P., Winemiller, K.O. (2003). Effects of 1997–1998 El Niño on the dynamics of the shallow-water fish assemblage of the Patos Lagoon Estuary (Brazil). *Estuar. Coast. Shelf Sci.* 57, 489–500, [http://dx.doi.org/10.1016/S0272-7714\(02\)00382-7](http://dx.doi.org/10.1016/S0272-7714(02)00382-7)

Garvine, R. (1975). The distribution of salinity and temperature in the Connecticut River Estuary. *Journal of Geophysical Research*, 80 (9), 1176-1183.

Geyer, W.R., Hill, P.S., Kineke, G.C. (2004). The transport, transformation and dispersal of sediment by buoyant coastal flows. *Cont. Shelf Res.* 24, 927–949

Gong, W; Shen, J. (2011). The response of salt intrusion to changes in river discharge and tidal mixing during the dry season in the Modaomen Estuary, China. *Continental Shelf Research*, 31, 769-788.

Grimm, A. M., Tedeschi, R. G. (2009). ENSO and Extreme Rainfall Events in South America. *Journal of Climate*, v. 22, 1589-1609.

Hartmann, C. (1996) Dinâmica, distribuição e composição do material em suspensão na região sul da Laguna dos Patos, RS. Curso de Pós-Graduação em Geociências. Porto Alegre, UFRGS. Doutorado, 363.

Hervouet, J-M. (2007). Free surface flows: Modelling with the finite element methods. John Wiley & Sons Ltd, England.

Horowitz, A. J. (2003). An evaluation of sediment rating curves for estimating suspended sediment concentrations for subsequent flux calculations. *Hydrological Processes*, 17(17), 3387–3409. <https://doi.org/10.1002/hyp.1299>.

Kjerfve, B. (1986). Circulation and Salt Flux in a Well Mixed Estuary. Em: VAN de KREEKE, J. (ed.). *Physics of Shallow Estuaries and Bays*. Berlin, Springer-Verlag, 22–29 p.

Krajewski, A., Sikorska, A. E. and Banasik, K. (2017) Modeling Suspended Sediment Concentration in the Stormwater Outflow from a Small Detention Pond, *Journal of Environmental Engineering (United States)*, 143(10), pp. 1–11. doi: 10.1061/(ASCE)EE.1943-7870.0001258.

Lihan, T., Saitoh, S., Iida, T., Hirawake, T., Iida, K. (2008) 'Satellite-measured temporal and spatial variability of the Tokachi River plume', *Estuarine, Coastal and Shelf Science*, 78(2), pp. 237–249. doi: 10.1016/j.ecss.2007.12.001.

Lopes, J.F., Dias, J.M., Dekeyser, I. (2006). Numerical modeling of cohesive sediments transport in the Ria de Aveiro lagoon, Portugal. *Journal of Hydrology*, 319, pp. 176-198.

- Lumborg, U. and Pejrup, M. (2005). Modelling of cohesive sediment transport in a tidal lagoon - An annual budget, *Marine Geology*, 218(1–4), pp. 1–16. doi: 10.1016/j.margeo.2005.03.015.
- Lumborg, U. and Windelin, A. (2003). Hydrography and cohesive sediment modelling: application to the RømøDyb tidal area, *Journal of Marine Systems*, 38(3–4), pp. 287–303. doi: 10.1016/S0924-7963(02)00247-6.
- Marques, W. C., Fernandes, E. H., Moraes, B. C., Moller, O. O., Malcherek, A. (2010). Dynamics of the Patos Lagoon coastal plume and its contribution to the deposition pattern of the southern Brazilian inner shelf, *Journal of Geophysical Research: Oceans*, 115(10), pp. 1–22. doi: 10.1029/2010JC006190.
- Marques, W. C. (2012). The Temporal Variability of the Freshwater Discharge and Water Levels at the Patos Lagoon, Brazil. *International Journal of Geosciences*, v. 3, p. 758-766.
- Marques, W. C., Stringari, C. E. & Eidt, R. T. (2014). The Exchange Processes of the Patos Lagoon Estuary – Brazil: A Typical El Niño Year versus a Normal Meteorological Conditions Year, *Advances in Water Resource and Protection (AWRP)*, p. 11-20.
- Meccia, V. L., Simionato, C. G., Guerrero, R. A. (2018). The Río de la Plata Estuary Response to Wind Variability in Synoptic Timescale: Salinity Fields and Salt Wedge Structure. *Journal of Coastal Research*, 29 (1), 61-77.
- Mendes, R., Saldias, G. S., deCastro, M., Gomez-Gesteira, M., Vaz, N., Dias, J. M. (2017). Seasonal and interannual variability of the Douro turbid river plume, northwestern Iberian Peninsula. *Remote Sensing of Environment*, v. 194, 401-411.
- Miller, R. L., & McKee, B. A. (2004). Using MODIS Terra 250 m imagery to map concentrations of total suspended matter in coastal waters. *Remote Sensing of Environment*, 93(1–2), 259–266. <https://doi.org/10.1016/j.rse.2004.07.012>.
- Milliman, J. D., Meade, R. H. (1983). World-wide Delivery of River Sediment to the Oceans. *The Journal of Geology*, 91(1), 1-21.
- Möller, O.; Lorenzetti, J.; Stech J.; Mata, M. (1996) The Summertime Circulation and Dynamics of Patos Lagoon. *Continental Shelf Research*, 16:355–351.
- Möller, O. O., Castaing, P., Salomon, J., Lazure, P. (2001). The Influence of Local and Non-Local Forcing Effects on the Subtidal Circulation of Patos Lagoon, *Estuaries*, 24(2), p. 297. doi: 10.2307/1352953.
- Möller, O. O., Castello, J. P. and Vaz, A. C. (2009) The effect of river discharge and winds on the interannual variability of the pink shrimp *Farfantepenaeus paulensis* production in Patos Lagoon', *Estuaries and Coasts*, 32(4), pp. 787–796. doi: 10.1007/s12237-009-9168-6.
- Oliveira, H. A., Fernandes, E. H. L., Möller, O. O. Collares, G. L. (2015). Processos Hidrológicos e Hidrodinâmicos da Lagoa Mirim. *Revista Brasileira de Recursos Hídricos*, v. 20, p. 34-45.
- Pagot, M., Rodriguez, A, Hillman, G, Corral, M., Orona, C., Niencheski, L. F. (2007) 'Remote Sensing Assessment of Suspended Matter and Dynamics in Patos Lagoon', *Journal of Coastal Research*, 10047(47), pp. 116–129. doi: 10.2112/1551-5036-



47.sp1.116.

Pasquini, A. I., Niencheski, L. F. H., Depetris, P. J. (2012). The ENSO signature and other hydrological characteristics in Patos and adjacent coastal lagoons, south-eastern Brazil. *Estuarine, Coastal and Shelf Science*, v. 111.

Petti, M.; Bosa, S; Pascolo, S. (2018). Lagoon Sediment Dynamics: A Coupled Model to Study a Medium-Term Silting of Tidal Channels. *Water* 10, no. 5: 569.

Portela, L. I., Ramos, S., Trigo-Teixeira, A. (2013). Effect of salinity on the settling velocity of fine sediments of a harbour basin. In: Conley, D.C, Masselink, G., Russel, P.E. and O'Hare, T.J. (eds.s), *Proceedings 12<sup>th</sup> International Coastal Symposium* (Plymouth, England), *Journal of Coastal Research*, Special Issue No. 65, pp. 1188-1193, ISSN 0749-0208.

Ruhl, C.; Schoellhamer, D. (2004). Spatial and temporal variability of suspended-sediment concentrations in a shallow estuarine environment. *San Francisco Estuary and Watershed Science* 2(2).

Santoro, P., Fossati, M., Tassi, P., Huybrechts, N., Bang, D. P. V., Piedra-Cueva, J. C. I. (2017). A coupled wave-current-sediment transport model for an estuarine system: Application to the Río de la Plata and Montevideo Bay. *Applied Mathematical Modelling*, 52, 107-130.

Seeliger, U. (2001). The Patos Lagoon Estuary, Brazil. p. 167-183 In: Seeliger, U; Kjerfve, B. (Eds). *Coastal Marine Ecosystems of Latin America*. 1° ed. New York, Estados Unidos: Springer Science & Business Media. 366p.

Seiler, L. M. N., Fernandes, E. H. L., Martins, F., Abreu, P. C. (2015). Evaluation of hydrologic influence on water quality variation in a coastal lagoon through numerical modeling. *Ecological Modelling*, 314, 44-61.

Silva, P., Lisboa, P.; Fernandes, E. (2015). Changes on the fine sediment dynamics after the Port of Rio Grande expansion. *Advances in Geosciences*, v. 39, p. 123-127.

Sun C, Shimizu K, Symonds G. (2016). Numerical modelling of dredge plumes: a review. Report of Theme 3 - Project 3.1.3, prepared for the Dredging Science Node, Western Australian Marine Science Institution, Perth, Western Australia, 55 pp.

Toldo Jr., E.; Dillenburg, S.; Corrêa, I.; Almeida, L.; Weschenfelder, J.; Gruber, N. (2006). Sedimentação de Longo e Curto Período na Lagoa Dos Patos, Sul do Brasil. *Geociências*, 33(2):79-86.

Torrence, C.; Compo, G. (1998). A practical guide to wavelet analysis. *Bulletin of the American Meteorological Society*, v. 79, n.1, p.61-78.

Van Leussen, W. (1994). Estuarine macroflocs and their role in fine-grained transport. Thesis of doctorate, Universiteit Utrecht, Netherlands. 488p.

Van Leussen, W. 1999. The variability of settling velocities of suspended fine-grained sediment in the Ems estuary. *Journal of Sea Research*, 41(1-2), 109–118. doi:10.1016/s1385-1101(98)00046-x

Vantrepotte, V., Loisel, H., Meriaux, X., Neukermans, G., Dessailly, D., Jamet, C., Gensac, E., Gardel., A. (2011). Seasonal and inter-annual (2002-2010) variability of the suspended particulate matter as retrieved from satellite ocean color sensor over the

French Guiana coastal waters, *Journal of Coastal Research*, (64), pp. 1750–1754. doi: 0749-0208.

Vaz, A. C., Möller Jr., O. O. and de Almeida., T. L. (2006). Análise quantitativa da descarga dos rios afluentes da Lagoa dos Patos, *Atlântica*, 28(1), pp. 13–23. Available at: <http://www.lei.furg.br/atlantica/vol28/Numero1/ATL03.PDF>.

Villaret, C., Hervouet, J., Kopmann, R, Merkel, U., Davier, A. (2013). Morphodynamic modeling using the Telemac finite-element system, *Computers and Geosciences*. Elsevier, 53(April), pp. 105–113. doi: 10.1016/j.cageo.2011.10.004.

Villaret,C.; Trowbridge;J. (1991). Effects of stratification by suspended sediments on turbulent shear flows, *J. Geophys. Res.*, 96(C6), 10659–10680.

Walstra, L.; Van Rijn, L; Blogg, H.; Van Ormondt, M. (2001). Evaluation of a hydrodynamic area model based on the COAST3D data at Teignmouth 1999. Report TR121-EC MAST Project No. MAS3-CT97-0086, HR Wallingford, UK, Pp. D4.1-D4.4.

Wang, X; Pinard, V; Malacic, V. (2007). Sediment transport and resuspension due to combined motion of wave and current in the northern Adriatic Sea during a Bora event in January 2001: A numerical modelling study. *Continental Shelf Research*, 27, 613-633.